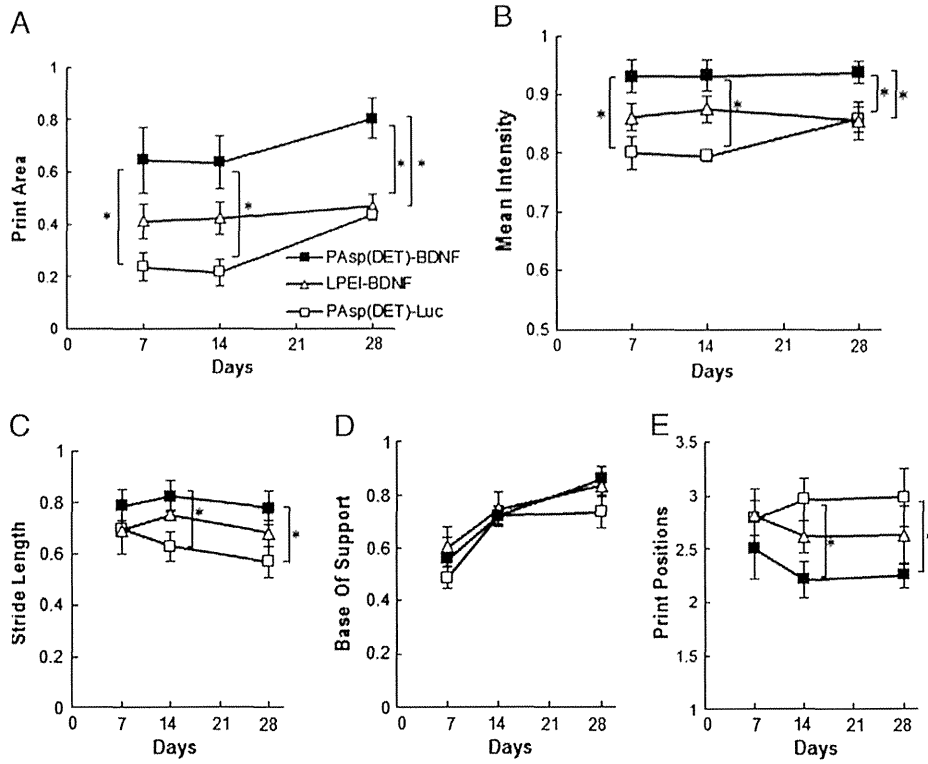

Fig. 4. Analysis of walking motion by CatWalk system. The parameters listed in Table 1 were evaluated; (A) print area, (B) mean intensity, (C) Stride length of hindlimb, (D) Base of support in hindlimbs, and (E) Print positions. Data are relative values to the average of non-injured intact control, expressed as means ± SEMs ($n = 6$), $^*p < 0.05$.

luciferase expression level was still considerably higher than the background level 7 days after injection of PAsp(DET) polyplex ($4.91 \pm 0.73 \times 10^5$ photons/s in PAsp (DET), $n = 5$, $2.52 \pm 0.06 \times 10^4$ photons/s in untreated background mice, $n = 3$).

In Fig. 1A, the expression from PAsp(DET)/pDNA and LPEI/pDNA polyplexes was intensely observed at thoracic region. To investigate the polyplex distribution more in details, we injected trypan blue solution intrathecally between L4 and L5. The blue staining was widely distributed in the spinal canal but accumulated more intensely at thoracic level than the other parts of spine (Fig. S1A). The cross sections of thoracic spinal cord (Th9) obtained immediately after the injection revealed that the blue staining was localized in meninges (Fig. S1B). In addition, by injecting Cy5-labeled pDNA/PAsp(DET) polyplexes to evaluate the distribution histologically, the Cy5 signals were observed in meninges and partly in parenchyma for both immediately or 24 h after the injection (Fig. S2). These results well consistent with previous reports of injecting cationic polyplexes intrathecally [34,35]. Thus, it is strong suggested that the solution rapidly passed in the subarachnoid space and widely distributed in the spinal tissue. Since the accumulation at thoracic region was observed regardless of polyplex types, it is reasonably assumed to be due to gravitational redistribution of fluid reflecting the spinal curvature.

Safety was investigated by analyzing proinflammatory cytokines after administration of PAsp(DET)/pDNA (luciferase) polyplexes into the SCI region in the mice receiving contusion at the level of the 9th thoracic vertebra (see Materials and Methods). The messenger RNA (mRNA) expression of TNF-α, IL-6, and IL-1β in the lower thoracic spinal cord region was significantly elevated with contusion; however, the intrathecal injection of the polyplex did not induce further cytokine production (Fig. 2A, B, C). Note that the injection did not affect the spontaneous recovery of motor function that was evaluated by BMS scoring for 4 weeks (Fig. 2D). Thus, it is confirmed that intrathecal injection of the polyplex provided sufficient transgene expression without harmful tissue injury and inflammation.

3.2. Therapeutic effect of BDNF-expressing pDNA on the recovery of walking motion

Using the PAsp(DET)/pDNA polyplex system, we applied BDNF-expressing pDNA for SCI mice. To evaluate the recovery of voluntary motor function, we did scoring of BMS and its subscore. This is a widely-used locomotor measurement with validity and reliability [31].

After administration of BDNF-expressing pDNA using PAsp(DET)/pDNA polyplexes, the BMS showed more rapid recovery compared with other controls of BDNF administration using LPEI/pDNA polyplexes, or negative control pDNA (luciferase) (Fig. 3A). The higher scores for PAsp(DET) polyplexes were obtained throughout the period from 3 to 28 days after administration of the polyplexes. In line with these results, the BMS subscore which reflects the footstep and its coordination showed remarkably higher scores for the mice receiving PAsp(DET)/pDNA polyplexes compared with the other controls after seven days of administration (Fig. 3B).

For a more detailed and quantitative assessment of walking motion, we did an analysis using the CatWalk system, which allows a comprehensive examination of walking motion by assessing the parameters shown in Table 1. These parameters are reported to precisely reflect the stepping coordination of the hindlimbs [36–38]. As shown in Fig. 4A–E, the mice receiving BDNF-expressing pDNA using the PAsp(DET)/pDNA polyplex generally showed early recovery compared with other groups. Among the parameters, "print area" and "mean intensity," representing the size and intensity of each footprint, showed significantly higher values one week after administration, suggesting

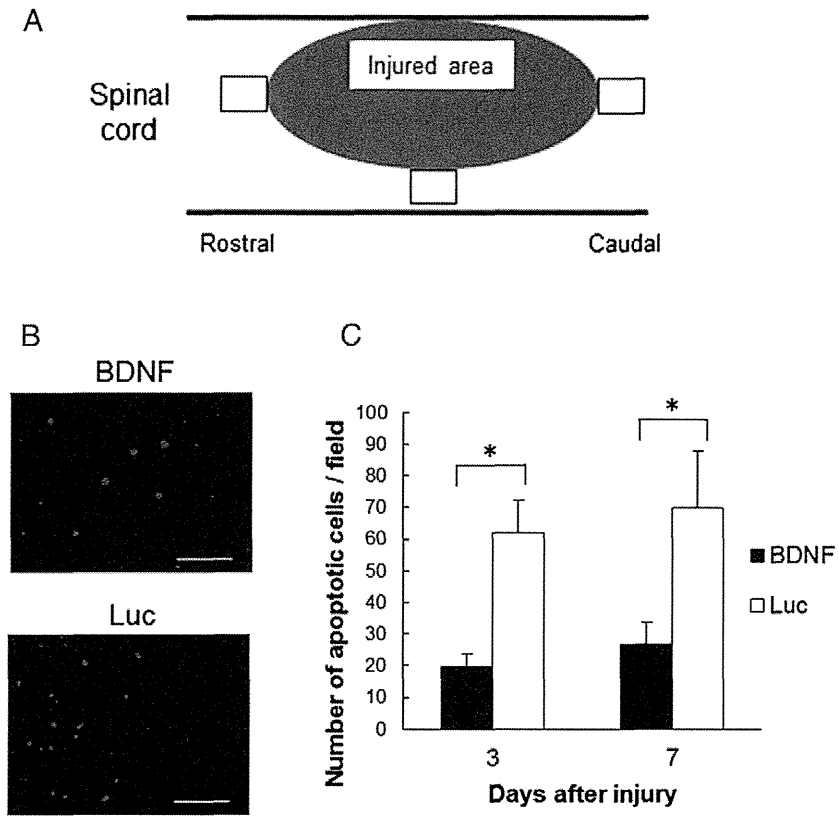

Fig. 5. Analysis of cell apoptosis by a TUNEL assay after experimental SCI. (A) Schematic representation for obtaining images for apoptotic cell counting. (B) Representative images of apoptotic cells that were labeled with TMR red around SCI region. Images were obtained under ×200 magnification using a fluorescence microscope (AxioVision: Carl Zeiss, Oberkochen, Germany) 3 days after induction of SCI and concomitant intrathecal injection of BDNF or luciferase-expressing pDNA using PAsp(DET). Scale bars represent 20 μm. (C) Counting of apoptotic cells from section images using image analyzer software (WinROOF: Mitani Co., Tokyo, Japan). Data are expressed as average cell number per image ± SEMs ($n = 6$), $^*p < 0.05$.

the early recovery of walking motion with sufficient weight bearing (Fig. 4A, B). Other parameters of "stride length" and "print positions," reflecting stepping pattern and coordination, needed 2 weeks to show significant differences between the PAsp(DET)/pDNA polyplex group and others. It is important to note is that there is an accuracy limitation in the latter two parameters especially during the early period of recovery because the stride length of the hind foot would be falsely measured once a footstep is missed. In any case, the significant differences in the parameters were observed up to 4 weeks after administration, strongly suggesting that the BDNF-expressing pDNA introduced by the PAsp(DET)/pDNA polyplex provided sustainable therapeutic effect on the recovery of walking for more than 4 weeks.

3.3. Therapeutic effect of BDNF-expressing pDNA on neural cell survival and preservation

To investigate the mechanisms of walking motion recovery, the neural cell survival was determined histologically in the injured spinal cord by the TUNEL assay to calculate the number of apoptotic cells (Fig. 5A). On days 3 and 7 after SCI, the number of TUNEL-positive (apoptotic) cells was significantly lower for the mice receiving BDNF-expressing pDNA using PAsp(DET)/pDNA polyplex compared with the control mice receiving luciferase-expressing pDNA (Fig. 5B, C). Since there was no difference in the total number of cells between these two groups, it is suggested that the BDNF-expressing pDNA effectively decreased apoptotic cell death in the injured spinal cord.

The size of damaged spinal cord tissue was evaluated in the injured spinal cord by Luxol fast blue (LFB) staining, a selective staining of myelinated axons. We analyzed five serial horizontal sections with the range of 400 μm rostrally and caudally from the epicenter of injury (Fig. 6A). As shown in Fig. 6B, the LFB-negative area indicating the damaged spinal cord was apparently smaller in the mice receiving BDNF-expressing pDNA compared with the control mice. The planimetry of the sections revealed that the BDNF provided neuroprotective effects in maintaining the axons in an intact myelinated state after SCI, displayed by the significantly increased LFB-positive areas in the sections of both rostral and caudal regions after 2 weeks of administration (Fig. 6C). It is reasonable to assume that the anti-apoptotic, neuroprotective effect in the nerve tissue contributed to the rapid recovery of walking motion as early as one week after administration (Fig. 4). On the other hand, at 4 weeks after administration, the significantly larger LFB-positive area was still observed in the BDNF group (Fig. 6D), strongly suggesting the sustained effect of BDNF-expressing pDNA. However, for BDNF and control groups, the rates of LFB positive area also showed higher values at 4 weeks compared with 2 weeks; thus, a certain degree of spontaneous motor function recovery should be included in the results.

4. Discussion

The aim of this study was to demonstrate the feasibility of the PAsp(DET)/pDNA polyplex system which can introduce genes with high efficacy and safety for the treatment of SCI. While a number of therapeutic agents including BDNF have been identified for SCI, there remains a severe problem of how to deliver these agents to the target region of the injured spinal cord. In the case of peptides and proteins, the effects tend to be too short due to limited duration in the tissues. Therefore, repeated administration or a sustained-release formulation

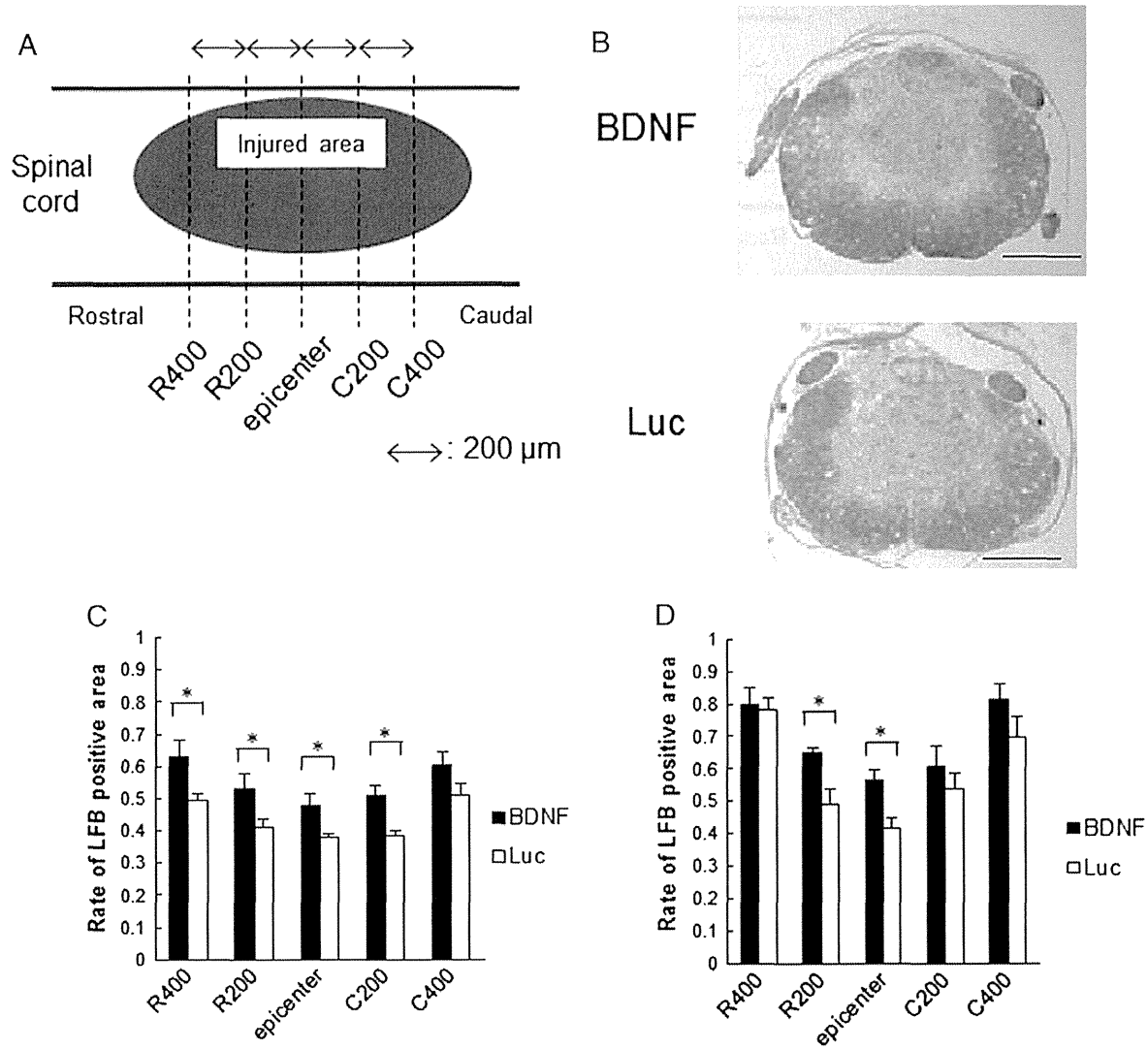

Fig. 6. Evaluation of tissue sparing after experimental SCI. (A) Scheme of evaluating the tissue sparing in the longitudinal sections of spinal cord. Transverse spinal cord sections were serially obtained from 400 μm rostral (R400) to 400 μm caudal (C400) to the epicenter with 200 μm intervals. (B) Representative images of transverse spinal cord sections at the epicenter with Luxol fast blue (LFB) staining, 2 weeks after SCI and concomitant intrathecal injection of BDNF or luciferase-expressing pDNA using PAsp(DET). Scale bars: 500 μm. (C, D) Quantification of LFB positive area 2 weeks (C) or 4 weeks (D) after SCI and the pDNA injection. Data are expressed as means ± SEMs ($n = 6$), $^*p < 0.05$.

is needed, but these techniques are likely to induce various complications such as scarring and secondary tissue damage [29,30,39].

Gene delivery is promising in overcoming these issues. Besides the sustained manner of protein production, the gene can express, in principle, any protein and peptide by modifying its base sequences. Thus, gene introduction potentially applies well to various situations in the complex pathology of SCI. When a secretary factor(s) is applied, the target cells for gene introduction would not be restricted to neural cells. Any cells surrounding the SCI region are capable of secreting the factor(s) into the region.

In this sense, the advantages of non-viral systems such as their safety and ease of preparation deserve attention for SCI treatment. We chose BDNF for the therapeutic agent of SCI. BDNF was discovered in the early 1980s and has been gaining particular interest among several neurotrophic factors because it promotes neuronal function and activity in the CNS [25,40–42]. BDNF has been tried recently in the treatment of SCI where diverse effects have been reported, including elongation of neural cell survival, promotion of axonal regeneration, plasticity, and re-myelination [26,43]. In acute SCI, BDNF exhibited anti-apoptotic effects on neurons and oligodendrocytes within 2 weeks after SCI with BDNF peptide-continuous infusion or transfection of a BDNF-expressing adenoviral vector [44–46].

We introduced BDNF-expressing pDNA into neural tissue using the PAsp(DET)/pDNA polyplex concomitantly with the induction of experimental SCI. As expected, BDNF protein expressed from the pDNA showed remarkable anti-apoptotic effects in neural cells (Fig. 5) and preservation of normally myelinated axons (Fig. 6). Eventually, walking function showed a remarkably early recovery. Compared with protein administration which shows very rapid clearance in CSF [29], pDNA was capable of providing transgene expression for more than a week, and it is reasonable to assume that BDNF-expressing pDNA was advantageous in managing the complex pathology of SCI that would last for more than several weeks.

It is interesting that the mice receiving BDNF by LPEI/pDNA polyplex also showed considerable recovery of motor function compared with the negative control mice treated with luciferase-expressing gene using PAsp(DET), although the degree of recovery was generally lower than that of the group receiving BDNF by PAsp(DET)/pDNA (Figs. 3 and 4).

The reason could be partly due to the difference in efficiency of transgene expression between PAsp(DET) and LPEI (Fig. 1B). Indeed, although LPEI is known to have high transfection efficiency due to its endosome-buffering capacity, PAsp(DET) has a more sophisticated manner of pH-selective membrane destabilization to disrupt endosomal membranes, resulting in more efficient gene introduction with smooth transport of the polyplexes into cytoplasm [21,47].

In addition, a critical problem about the safety of gene introduction should be raised; even after good transgene expression is obtained, cell viability may gradually decrease with fluctuations in endogenous gene expressions [24]. For example, despite the high efficiency of *in vitro* and even *in vivo* gene introduction, LPEI still has a problem of long-term safety mostly due to its non-degradability inside the cells, resulting in the regrettable fact that PEI has never been used for clinical purposes. On the other hand, other non-viral systems, especially lipid-based systems, generally have disadvantages in low efficiency of *in vivo* gene introduction compared with the remarkably high capacity for cultured cells in some cases, comparable to capacities of viral vectors [48,49]. Indeed, for SCI, there are few reports in animal studies showing sufficient improvement of neural function by introduction of therapeutic molecules, although a considerable number of systems achieved *in vitro* transgene expression in neural cells such as neurons and astrocytes [50].

PAsp(DET) is advantageous both in safety due to its spontaneous biodegradability into a non-toxic form, and high transfection efficiency due to the definite mechanism of endosome escape as mentioned previously. As a proof-of-concept study, it is demonstrated that the administration of BDNF-expressing pDNA using PAsp(DET) polyplexes provided high BDNF expression in an effective manner to enhance the motor function recovery after SCI. As far as we know, this is the first report of gene introduction using a non-viral system to confirm the improved neural function with extensive assessment of walking motion. The sustained effect of BDNF in protecting neural cell death, which lasted for a few weeks even after a single administration of BDNF-expressing pDNA, is likely to be attributed to the biocompatible manner of the PAsp(DET) system to minimize toxic effects that might hamper the recovery of neural function.

In conclusion, gene introduction into a spinal cord region using the PAsp(DET)/pDNA polyplex system provided sufficient transgene expression without harmful tissue injury and inflammation. For experimental SCI, the introduction of BDNF-expressing pDNA significantly enhanced the recovery of neural function with neuroprotective effects on neural cells in preventing cell death. We believe this approach has therapeutic use for treating spinal cord injury.

Supplementary data to this article can be found online at http://dx.doi.org/10.1016/j.jconrel.2014.10.027.

Acknowledgments

This work was financially supported in part by JSPS KAKENHI Grant-in-Aid for Scientific Research (B) (grant number 24300170 (K.I.)), the Center of Innovation (COI) Program and the S-innovation program from Japan Science and Technology Agency (JST), and the JSPS Core-to-Core Program, A. Advanced Research Networks. We thank Ms. Katsue Morii, Satomi Ogura, Asuka Miyoshi, and Sae Suzuki (The University of Tokyo) for technical assistance.

References

[1] S. Rossignol, M. Schwab, M. Schwartz, M.G. Fehlings, Spinal cord injury: time to move? J. Neurosci. 27 (2007) 11782–11792.
[2] A.K. Varma, A. Das, G.t. Wallace, J. Barry, A.A. Vertegel, S.K. Ray, N.L. Banik, Spinal cord injury: a review of current therapy, future treatments, and basic science frontiers, Neurochem. Res. 38 (2013) 895–905.
[3] M.S. Beattie, A.A. Farooqui, J.C. Bresnahan, Review of current evidence for apoptosis after spinal cord injury, J. Neurotrauma 17 (2000) 915–925.
[4] P.G. Popovich, Z. Guan, V. McGaughy, L. Fisher, W.F. Hickey, D.M. Basso, The neuropathological and behavioral consequences of intraspinal microglial/macrophage activation, J. Neuropathol. Exp. Neurol. 61 (2002) 623–633.
[5] C.A. Oyinbo, Secondary injury mechanisms in traumatic spinal cord injury: a nugget of this multiply cascade, Acta Neurobiol. Exp. 71 (2011) 281–299.
[6] M. Nakamura, B.S. Bregman, Differences in neurotrophic factor gene expression profiles between neonate and adult rat spinal cord after injury, Exp. Neurol. 169 (2001) 407–415.
[7] J. Widenfalk, K. Lundstromer, M. Jubran, S. Brene, L. Olson, Neurotrophic factors and receptors in the immature and adult spinal cord after mechanical injury or kainic acid, J. Neurosci. 21 (2001) 3457–3475.
[8] J.R. Bethea, W.D. Dietrich, Targeting the host inflammatory response in traumatic spinal cord injury, Curr. Opin. Neurol. 15 (2002) 355–360.
[9] S.P. Niclou, E.H. Franssen, E.M. Ehlert, M. Taniguchi, J. Verhaagen, Meningeal cell-derived semaphorin 3A inhibits neurite outgrowth, Mol. Cell. Neurosci. 24 (2003) 902–912.
[10] M.D. Benson, M.I. Romero, M.E. Lush, Q.R. Lu, M. Henkemeyer, L.F. Parada, Ephrin-B3 is a myelin-based inhibitor of neurite outgrowth, Proc. Natl. Acad. Sci. U. S. A. 102 (2005) 10694–10699.
[11] H.S. Sharma, New perspectives for the treatment options in spinal cord injury, Expert. Opin. Pharmacother. 9 (2008) 2773–2800.
[12] K. Kitamura, A. Iwanami, M. Nakamura, J. Yamane, K. Watanabe, Y. Suzuki, D. Miyazawa, S. Shibata, H. Funakoshi, S. Miyatake, R.S. Coffin, T. Nakamura, Y. Toyama, H. Okano, Hepatocyte growth factor promotes endogenous repair and functional recovery after spinal cord injury, J. Neurosci. Res. 85 (2007) 2332–2342.
[13] E. Marshall, Gene therapy death prompts review of adenovirus vector, Science 286 (1999) 2244–2245.
[14] M. Cavazzana-Calvo, S. Hacein-Bey, G. de Saint Basile, F. Gross, E. Yvon, P. Nusbaum, F. Selz, C. Hue, S. Certain, J.L. Casanova, P. Bousso, F.L. Deist, A. Fischer, Gene therapy of human severe combined immunodeficiency (SCID)-X1 disease, Science 288 (2000) 669–672.
[15] A. Fischer, S. Hacein-Bey-Abina, C. Lagresle, A. Garrigue, M. Cavazana-Calvo, Gene therapy of severe combined immunodeficiency disease: proof of principle of efficiency and safety issues. Gene therapy, primary immunodeficiencies, retrovirus, lentivirus, genome, Bull. Acad. Natl Med. 189 (2005) 779–785 (discussion 786-778).
[16] K. Itaka, K. Kataoka, Recent development of nonviral gene delivery systems with virus-like structures and mechanisms, Eur. J. Pharm. Biopharm. 71 (2009) 475–483.
[17] K. Itaka, K. Kataoka, Progress and prospects of polyplex nanomicelles for plasmid DNA delivery, Curr. Gene Ther. 11 (2011) 457–465.
[18] O. Boussif, F. Lezoualc'h, M.A. Zanta, M.D. Mergny, D. Scherman, B. Demeneix, J.P. Behr, A versatile vector for gene and oligonucleotide transfer into cells in culture and *in vivo*: polyethylenimine, Proc. Natl. Acad. Sci. U. S. A. 92 (1995) 7297–7301.
[19] S.M. Moghimi, P. Symonds, J.C. Murray, A.C. Hunter, G. Debska, A. Szewczyk, A two-stage poly(ethylenimine)-mediated cytotoxicity: implications for gene transfer/therapy, Mol. Ther. 11 (2005) 990–995.
[20] N. Kanayama, S. Fukushima, N. Nishiyama, K. Itaka, W.D. Jang, K. Miyata, Y. Yamasaki, U.I. Chung, K. Kataoka, A PEG-based biocompatible block catiomer with high buffering capacity for the construction of polyplex micelles showing efficient gene transfer toward primary cells, ChemMedChem 1 (2006) 439–444.
[21] K. Miyata, N. Nishiyama, K. Kataoka, Rational design of smart supramolecular assemblies for gene delivery: chemical challenges in the creation of artificial viruses, Chem. Soc. Rev. 41 (2012) 2562–2574.
[22] K. Itaka, T. Ishii, Y. Hasegawa, K. Kataoka, Biodegradable polyamino acid-based polycations as safe and effective gene carrier minimizing cumulative toxicity, Biomaterials 31 (2010) 3707–3714.
[23] K. Itaka, S. Ohba, K. Miyata, H. Kawaguchi, K. Nakamura, T. Takato, U.I. Chung, K. Kataoka, Bone regeneration by regulated *in vivo* gene transfer using biocompatible polyplex nanomicelles, Mol. Ther. 15 (2007) 1655–1662.
[24] K. Masago, K. Itaka, N. Nishiyama, U.I. Chung, K. Kataoka, Gene delivery with biocompatible cationic polymer: pharmacogenomic analysis on cell bioactivity, Biomaterials 28 (2007) 5169–5175.
[25] Y.A. Barde, D. Edgar, H. Thoenen, Purification of a new neurotrophic factor from mammalian brain, EMBO J. 1 (1982) 549–553.
[26] N. Weishaupt, A. Blesch, K. Fouad, BDNF: the career of a multifaceted neurotrophin in spinal cord injury, Exp. Neurol. 238 (2012) 254–264.
[27] L. Novikov, L. Novikova, J.O. Kellerth, Brain-derived neurotrophic factor promotes axonal regeneration and long-term survival of adult rat spinal motoneurons *in vivo*, Neuroscience 79 (1997) 765–774.
[28] A. Kishino, Y. Ishige, T. Tatsuno, C. Nakayama, H. Noguchi, BDNF prevents and reverses adult rat motor neuron degeneration and induces axonal outgrowth, Exp. Neurol. 144 (1997) 273–286.
[29] F. Dittrich, G. Ochs, A. Grosse-Wilde, U. Berweiler, Q. Yan, J.A. Miller, K.V. Toyka, M. Sendtner, Pharmacokinetics of intrathecally applied BDNF and effects on spinal motoneurons, Exp. Neurol. 141 (1996) 225–239.
[30] L.L. Jones, M.H. Tuszynski, Chronic intrathecal infusions after spinal cord injury cause scarring and compression, Microsc. Res. Tech. 54 (2001) 317–324.
[31] D.M. Basso, L.C. Fisher, A.J. Anderson, L.B. Jakeman, D.M. McTigue, P.G. Popovich, Basso Mouse Scale for locomotion detects differences in recovery after spinal cord injury in five common mouse strains, J. Neurotrauma 23 (2006) 635–659.
[32] J. Schira, M. Gasis, V. Estrada, M. Hendricks, C. Schmitz, T. Trapp, F. Kruse, G. Kogler, P. Wernet, H.P. Hartung, H.W. Muller, Significant clinical, neuropathological and behavioural recovery from acute spinal cord trauma by transplantation of a well-defined somatic stem cell from human umbilical cord blood, Brain 135 (2012) 431–446.
[33] H. Kluver, E. Barrera, A method for the combined staining of cells and fibers in the nervous system, J. Neuropathol. Exp. Neurol. 12 (1953) 400–403.

[34] L. Shi, G.P. Tang, S.J. Gao, Y.X. Ma, B.H. Liu, Y. Li, J.M. Zeng, Y.K. Ng, K.W. Leong, S. Wang, Repeated intrathecal administration of plasmid DNA complexed with polyethylene glycol-grafted polyethylenimine led to prolonged transgene expression in the spinal cord, Gene Ther. 10 (2003) 1179–1188.
[35] G.P. Tang, H.Y. Guo, F. Alexis, X. Wang, S. Zeng, T.M. Lim, J. Ding, Y.Y. Yang, S. Wang, Low molecular weight polyethylenimines linked by beta-cyclodextrin for gene transfer into the nervous system, J. Gene Med. 8 (2006) 736–744.
[36] F.P. Hamers, A.J. Lankhorst, T.J. van Laar, W.B. Veldhuis, W.H. Gispen, Automated quantitative gait analysis during overground locomotion in the rat: its application to spinal cord contusion and transection injuries, J. Neurotrauma 18 (2001) 187–201.
[37] F.P. Hamers, G.C. Koopmans, E.A. Joosten, CatWalk-assisted gait analysis in the assessment of spinal cord injury, J. Neurotrauma 23 (2006) 537–548.
[38] S. van Gorp, M. Leerink, O. Kakinohana, O. Platoshyn, C. Santucci, J. Galik, E.A. Joosten, M. Hruska-Plochan, D. Goldberg, S. Marsala, K. Johe, J.D. Ciacci, M. Marsala, Amelioration of motor/sensory dysfunction and spasticity in a rat model of acute lumbar spinal cord injury by human neural stem cell transplantation, Stem Cell Res. Ther. 4 (2013) 57.
[39] H. Terada, T. Kazui, M. Takinami, K. Yamashita, N. Washiyama, B.A. Muhammad, Reduction of ischemic spinal cord injury by dextrorphan: comparison of several methods of administration, J. Thorac. Cardiovasc. Surg. 122 (2001) 979–985.
[40] J.E. Johnson, Y.A. Barde, M. Schwab, H. Thoenen, Brain-derived neurotrophic factor supports the survival of cultured rat retinal ganglion cells, J. Neurosci. 6 (1986) 3031–3038.
[41] A.H. Nagahara, D.A. Merrill, G. Coppola, S. Tsukada, B.E. Schroeder, G.M. Shaked, L. Wang, A. Blesch, A. Kim, J.M. Conner, E. Rockenstein, M.V. Chao, E.H. Koo, D. Geschwind, E. Masliah, A.A. Chiba, M.H. Tuszynski, Neuroprotective effects of brain-derived neurotrophic factor in rodent and primate models of Alzheimer's disease, Nat. Med. 15 (2009) 331–337.
[42] A.H. Nagahara, M.H. Tuszynski, Potential therapeutic uses of BDNF in neurological and psychiatric disorders, Nat. Rev. Drug Discov. 10 (2011) 209–219.
[43] D.R. Kaplan, F.D. Miller, Neurotrophin signal transduction in the nervous system, Curr. Opin. Neurobiol. 10 (2000) 381–391.
[44] M. Koda, M. Murakami, H. Ino, K. Yoshinaga, O. Ikeda, M. Hashimoto, M. Yamazaki, C. Nakayama, H. Moriya, Brain-derived neurotrophic factor suppresses delayed apoptosis of oligodendrocytes after spinal cord injury in rats, J. Neurotrauma 19 (2002) 777–785.
[45] H. Nakajima, K. Uchida, T. Yayama, S. Kobayashi, A.R. Guerrero, S. Furukawa, H. Baba, Targeted retrograde gene delivery of brain-derived neurotrophic factor suppresses apoptosis of neurons and oligodendroglia after spinal cord injury in rats, Spine (Phila Pa 1976) 35 (2010) 497–504.
[46] Q. Chen, K. Osada, T. Ishii, M. Oba, S. Uchida, T.A. Tockary, T. Endo, Z. Ge, H. Kinoh, M.R. Kano, K. Itaka, K. Kataoka, Homo-catiomer integration into PEGylated polyplex micelle from block-catiomer for systemic anti-angiogenic gene therapy for fibrotic pancreatic tumors, Biomaterials 33 (2012) 4722–4730.
[47] K. Miyata, M. Oba, M. Nakanishi, S. Fukushima, Y. Yamasaki, H. Koyama, N. Nishiyama, K. Kataoka, Polyplexes from poly(aspartamide) bearing 1,2-diaminoethane side chains induce pH-selective, endosomal membrane destabilization with amplified transfection and negligible cytotoxicity, J. Am. Chem. Soc. 130 (2008) 16287–16294.
[48] G. Chen, Y. Ito, S. Masuda, R. Sasaki, Growth and secretion of erythropoietin of Chinese hamster ovary cells coexpressing epidermal growth factor receptor and erythropoietin genes: design of cells for cell culture matrix, Cytotechnology 35 (2001) 3–8.
[49] T. Higashi, I.A. Khalil, K.K. Maiti, W.S. Lee, H. Akita, H. Harashima, S.K. Chung, Novel lipidated sorbitol-based molecular transporters for non-viral gene delivery, J. Control. Release 136 (2009) 140–147.
[50] L. Yao, S. Yao, W. Daly, W. Hendry, A. Windebank, A. Pandit, Non-viral gene therapy for spinal cord regeneration, Drug Discov. Today 17 (2012) 998–1005.

Precise Engineering of siRNA Delivery Vehicles to Tumors Using Polyion Complexes and Gold Nanoparticles

Hyun Jin Kim,[†] Hiroyasu Takemoto,[‡] Yu Yi,[§] Meng Zheng,[⊥] Yoshinori Maeda,[§] Hiroyuki Chaya,[⊥] Kotaro Hayashi,[§] Peng Mi,[‡] Frederico Pittella,[⊥] R. James Christie,[⊥] Kazuko Toh,[⊥] Yu Matsumoto,[⊥] Nobuhiro Nishiyama,[‡] Kanjiro Miyata,[⊥,*] and Kazunori Kataoka[†,§,⊥,∥,*]

[†]Department of Materials Engineering, Graduate School of Engineering, The University of Tokyo, Tokyo 113-8656, Japan, [‡]Polymer Chemistry Division, Chemical Resources Laboratory, Tokyo Institute of Technology, Yokohama 226-8503, Japan, [§]Department of Bioengineering, Graduate School of Engineering, The University of Tokyo, Tokyo 113-8656, Japan, [⊥]Center for Disease Biology and Integrative Medicine, Graduate School of Medicine, The University of Tokyo, Tokyo 113-0033, Japan, and [∥]Center for NanoBio Integration, The University of Tokyo, Tokyo 113-8656, Japan

ABSTRACT For systemic delivery of siRNA to solid tumors, a size-regulated and reversibly stabilized nanoarchitecture was constructed by using a 20 kDa siRNA-loaded unimer polyion complex (uPIC) and 20 nm gold nanoparticle (AuNP). The uPIC was selectively prepared by charge-matched polyionic complexation of a poly(ethylene glycol)-*b*-poly(L-lysine) (PEG-PLL) copolymer bearing ~40 positive charges (and thiol group at the ω-end) with a single siRNA bearing 40 negative charges. The thiol group at the ω-end of PEG-PLL further enabled successful conjugation of the uPICs onto the single AuNP through coordinate bonding, generating a nanoarchitecture (uPIC-AuNP) with a size of 38 nm and a narrow size distribution. In contrast, mixing thiolated PEG-PLLs and AuNPs produced a large aggregate in the absence of siRNA, suggesting the essential role of the preformed uPIC in the formation of nanoarchitecture. The smart uPIC-AuNPs were stable in serum-containing media and more resistant against heparin-induced counter polyanion exchange, compared to uPICs alone. On the other hand, the treatment of uPIC-AuNPs with an intracellular concentration of glutathione substantially compromised their stability and triggered the release of siRNA, demonstrating the reversible stability of these nanoarchitectures relative to thiol exchange and negatively charged AuNP surface. The uPIC-AuNPs efficiently delivered siRNA into cultured cancer cells, facilitating significant sequence-specific gene silencing without cytotoxicity. Systemically administered uPIC-AuNPs showed appreciably longer blood circulation time compared to controls, *i.e.*, bare AuNPs and uPICs, indicating that the conjugation of uPICs onto AuNP was crucial for enhancing blood circulation time. Finally, the uPIC-AuNPs efficiently accumulated in a subcutaneously inoculated luciferase-expressing cervical cancer (HeLa-Luc) model and achieved significant luciferase gene silencing in the tumor tissue. These results demonstrate the strong potential of uPIC-AuNP nanoarchitectures for systemic siRNA delivery to solid tumors.

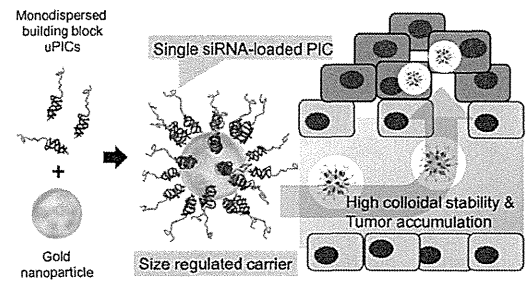

KEYWORDS: siRNA delivery · unimer polyion complex · gold nanoparticle · cancer therapy

Small interfering RNA (siRNA), which induces the sequence-specific degradation of mRNA in the cytoplasm (termed RNA interference (RNAi)), has attracted much attention in cancer therapy.[1,2] However, systemically administered siRNA is rapidly degraded by RNases in the bloodstream and/or eliminated through kidney filtration because they are smaller than 6 nm.[3,4] Thus, siRNA carriers need to be developed in order to overcome these issues for successful therapy. A variety of synthetic nanocarriers have been constructed mainly with cationic nanomaterials, such as lipids, polycations, inorganic nanoparticles, and their hybrid systems.[5−10] These nanocarriers can protect siRNA from enzymatic degradations and apparently increase its size to circumvent kidney filtration. This allows the siRNA payloads to accumulate in tumor tissues through the leaky tumor vasculature *via* the so-called enhanced permeability and retention (EPR) effect.[11,12] In this regard, several recent studies have revealed that precise size-tuning promotes the selective accumulation of nanoparticles in tumor tissues.[13,14] Nanoparticles with a size that is smaller than 50 nm can efficiently

* Address correspondence to kataoka@bmw.t.u-tokyo.ac.jp, miyata@bmw.t.u-tokyo.ac.jp.

Received for review April 17, 2014 and accepted August 18, 2014.

Published online August 18, 2014
10.1021/nn502125h

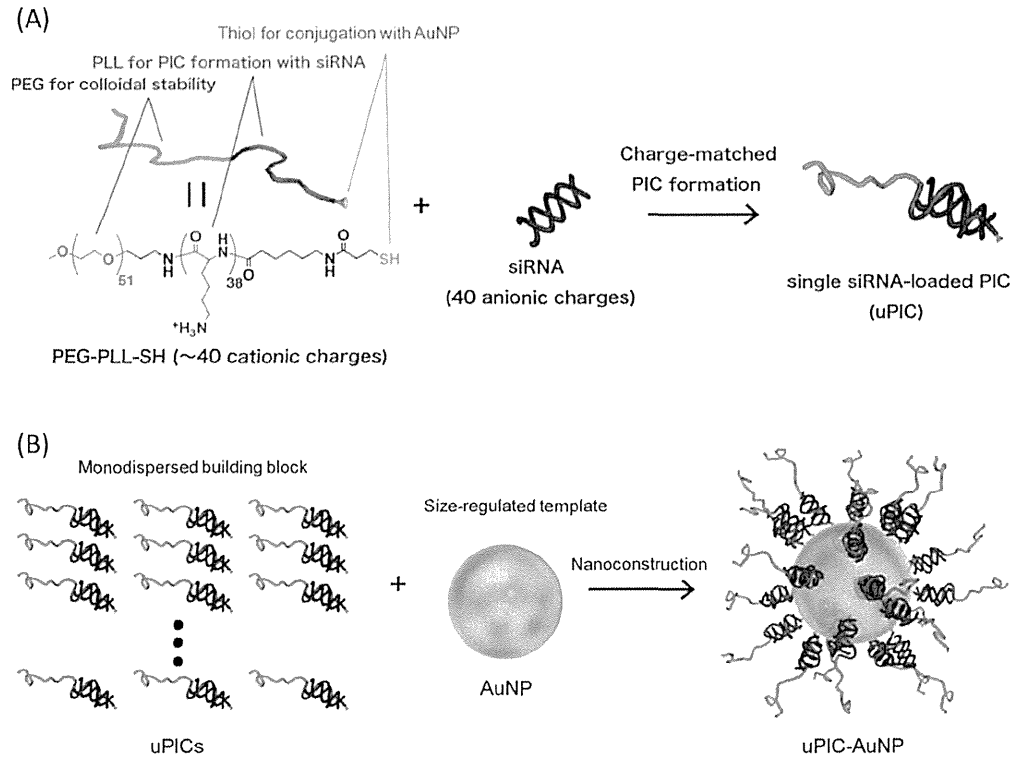

Figure 1. Schematic illustration showing the nanoconstruction of uPIC-AuNPs from monodispersed building blocks. (A) Formation of uPICs comprising a single pair of PEG-PLL and siRNA. (B) Thiol-gold coordination complex between uPICs and AuNP.

accumulate in tumor tissues, especially in a poorly permeable pancreatic tumor model.[13] Thus, the size of nanocarriers is important for enhancing siRNA accumulation in a variety of tumor tissues.

While multimolecular self-assemblies of siRNA with oppositely charged nanomaterials have been widely developed because of their facile and efficient encapsulation of siRNA, it is difficult to control the size and the distribution of these carriers. In contrast, the bottom-up nanocarrier construction with monodispersed building blocks and a nanotemplate enables more precise size-tuning at the nanoscale. With regard to such building blocks, our recent study demonstrated that a block copolymer of poly(ethylene glycol) and poly(L-lysine) (PEG-PLL) with a controlled degree of polymerization of PLL (DP_{PLL}) formed a unimer polyion complex (uPIC)[15] comprising a single siRNA molecule,[16,17] potentially serving as a monodispersed building block. A building-block-loading nanotemplate is necessary to satisfy the Janus-type property requirement for the selective siRNA release into the cytosol. Gold nanoparticles (AuNPs) are promising biocompatible nanotemplates, as their size can be precisely controlled with a narrow distribution, and also they can be coated with polymers or biomolecules through thiol chemistry.[18,19] This type of bonding is relatively stable under extracellular conditions, but these polymers or biomolecules can be competed off the AuNP with glutathione (GSH), which is abundant in the cytosol.[20] Subsequently, the GSH-coordinated anionic AuNPs may interact with uPICs to destabilize them for triggered siRNA release.

To achieve an efficient systemic siRNA delivery to solid tumors, we developed a size-regulated and reversibly stabilized nanoarchitecture (uPIC-AuNP) by utilizing an AuNP template and a monodispersed uPIC building block prepared with a single siRNA/PEG-PLL pair (Figure 1). To this end, a PEG-PLL was prepared to have a DP_{PLL} of ~40 (matched with the negative charges of 21mer/21mer siRNA) and thiol groups at the ω-end of PLL for coordinate bonding with AuNP. After confirming stable binding between single siRNA molecules and copolymers, the resulting uPICs were conjugated to a 20 nm AuNP to build uPIC-AuNP nanoarchitectures exhibiting sizes less than 50 nm and narrow size distributions under biological conditions. The uPIC-AuNPs achieved efficient siRNA accumulation in a subcutaneous tumor model by systemic administration and successfully induced sequence-specific gene silencing in the tumor tissue.

RESULTS AND DISCUSSION

Preparation and Characterizations of uPICs Comprising a Single PEG-PLL/siRNA Pair. PEG-PLL synthesis was targeted to possess 40 positive charges (or DP_{PLL} = 40), as it can complementarily neutralize the negative charges

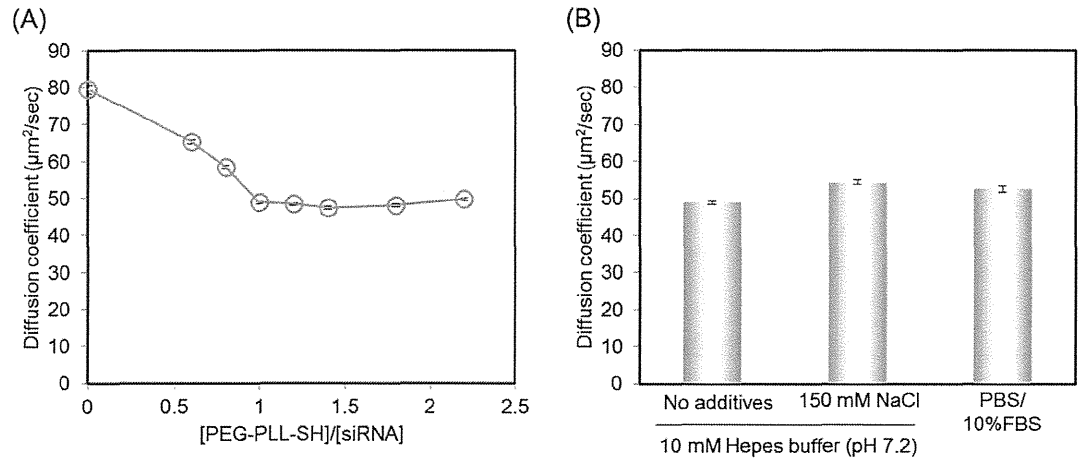

Figure 2. (A) Change in the diffusion coefficient of Cy3-siRNA upon polyionic complexation with PEG-PLL-SH in 10 mM Hepes buffer (pH 7.2) (Cy3-siRNA concentration = 10 nM). Results are expressed as mean and standard deviation (n = 10). (B) Diffusion coefficients of Cy3-siRNA-containing PICs prepared at [PEG-PLL-SH]/[siRNA] = 1.0 in various media (Cy3-siRNA concentration = 10 nM). Results are expressed as mean and standard deviation (n = 10).

of single 21mer/21mer siRNA and form uPICs through charge-matched polyionic complexation (Figure 1). The obtained PEG-PLL with TFA protective groups (PEG-PLL(TFA)) was determined to possess the DP_{PLL} of 38 in ^{1}H NMR spectrum (data not shown). The primary amine in the ω-end of PEG-PLL(TFA) was further modified with LC-SPDP for thiol-gold coordinate bonding, and the quantitative introduction of LC-SPDP was confirmed in ^{1}H NMR spectrum (Figure S1, Supporting Information (SI)). After successive removals of TFA and pyridyl groups with sodium hydroxide and dithiothreitol (DTT), respectively, the thiolated PEG-PLL (PEG-PLL-SH) was mixed with Cy3-labeled siRNA (Cy3-siRNA) at varying mixing ratios in 10 mM Hepes buffer (pH 7.2), and then characterized by fluorescence correlation spectroscopy (FCS). Note that FCS can determine a diffusion coefficient (D) of highly dilute fluorescent molecules even in serum-containing media.[21,22] The D values of PEG-PLL-SH/Cy3-siRNA mixtures decreased progressively with a molar ratio of PEG-PLL-SH to siRNA ([PEG-PLL-SH]/[siRNA]) and leveled off at [PEG-PLL-SH]/[siRNA] = 1 (Figure 2A). The initial decrease in the D indicates PIC formation between Cy3-siRNA and PEG-PLL-SH. The following plateau region in the D strongly suggests that all the Cy3-siRNAs were complexed with PEG-PLL-SH at [PEG-PLL-SH]/[siRNA] = 1, and an excess amount of PEG-PLL-SH at [PEG-PLL-SH]/[siRNA] > 1 did not bind to siRNA. The PIC prepared at [PEG-PLL-SH]/[siRNA] = 1 was further characterized by analytical ultracentrifugation (AUC) based on the absorbance at 260 nm for a precise structural determination. The molecular weight (MW) of PICs in 10 mM Hepes buffer (pH 7.2) containing 150 mM NaCl was calculated by combining the AUC (sedimentation equilibrium) data with a partial specific volume (PSV) of PICs (0.602 cm^3/g) and the buffer density (1.005 cm^3/g). Note that the PSV of PICs was determined as a mass average of PSV of siRNA (0.508 cm^3/g) and PSV of PEG-PLL (0.753 cm^3/g). The major parameters used for the calculation of MW of PICs are summarized in Table S1 (SI). The PIC exhibited a MW of approximately 22 kDa, consistent with the formation of a uPIC comprising a single pair of PEG-PLL (MW = 7200 Da) and siRNA (MW = 13 300 Da). Single siRNA loading in uPIC was confirmed by using FCS. The association number of siRNA in the PIC was determined to be 0.9 ± 0.1 using 10 nM Cy3-siRNA. It was calculated by normalizing the fluorescent particle number (or amplitude number particle) of the PIC to that of naked siRNA. Note that the diffusion coefficient of uPICs determined at 10 nM siRNA (~50 μm^2/sec) was maintained even at much higher concentrations, *i.e.*, 20 and 40 μM siRNA (Table S2 (SI)), indicating that the similar uPICs were also prepared under the preparation condition of uPIC-AuNPs (17 μM siRNA). The uPIC formation with a single pair of siRNA and PEG-PLL (DP of PLL = ~40) can be further validated from the standpoint of their molecular structures. Considering the fact that siRNA adopts a right-handed A-form helix with 11 bp per helical turn, a helical pitch of 2.8 nm, and a diameter of 2.3 nm,[23] PLL segment having the maximum main chain length of 4.1 nm per 11 amino acids and the maximum side chain length of 0.65 nm can completely make ion pairs with siRNA phosphates along the helical structure. Nevertheless, the complete ion pair formation between siRNA and PLL remains to be evidenced in further studies. The stability of uPICs prepared at [PEG-PLL-SH]/[siRNA] = 1 was further investigated by FCS (Figure 2B). The addition of 10% fetal bovine serum (FBS) and a physiological salt hardly affected the D values of the uPICs, indicating stable PIC formation under the biological conditions. These results demonstrated that the stable uPICs were selectively prepared using

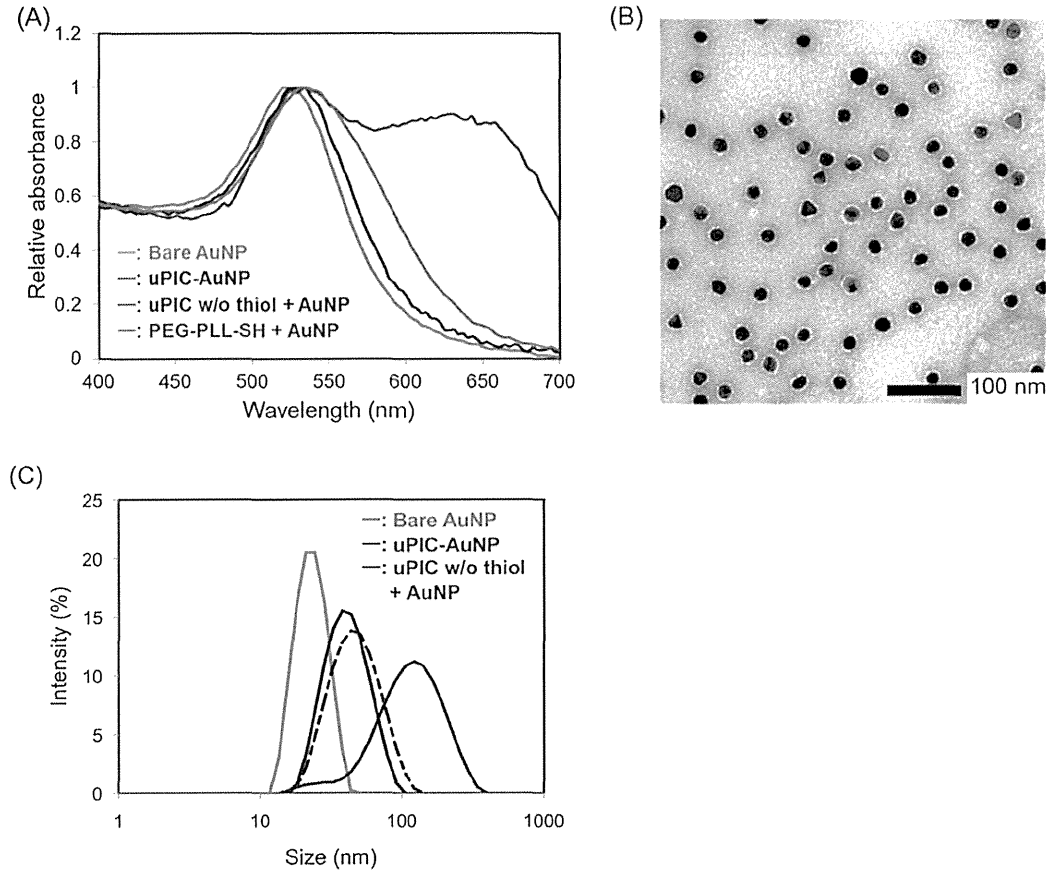

Figure 3. (A) UV–vis absorbance spectra of various sample solutions. Bare AuNP: AuNPs without PICs in 10 mM Hepes buffer (pH 7.2), uPIC-AuNP: uPIC-loaded AuNPs in 10 mM Hepes (pH 7.2) containing 150 mM NaCl, uPIC w/o thiol + AuNP: the mixture of AuNPs and uPICs prepared with nonthiolated PEG-PLL in 10 mM Hepes (pH 7.2) containing 150 mM NaCl, and PEG-PLL-SH + AuNP: the mixture of AuNPs and thiolated PEG-PLL without siRNA. (B) TEM image of uPIC-AuNPs. (C) Intensity-based DLS histograms of various sample solutions. Bare AuNP: AuNPs without PICs in 10 mM Hepes buffer (pH 7.2), uPIC-AuNP: uPIC-loaded AuNPs in 10 mM Hepes (pH 7.2) containing 150 mM NaCl (solid line) or 10% FBS (dashed line), and uPIC w/o thiol + AuNP: the mixture of AuNPs and uPICs prepared with nonthiolated PEG-PLL in 10 mM Hepes (pH 7.2) containing 150 mM NaCl. All samples were incubated overnight at ambient temperature (AuNP concentration: 12 nM).

PEG-PLL bearing ~40 positive charges, allowing their use as monodispersed building blocks for nanoconstruction.

Preparation and Characterizations of the Smart uPIC-AuNP Nanoarchitecture. uPICs were used as monodispersed building blocks for the construction of smart uPIC-AuNP nanoarchitectures (Figure 1). Specifically, the uPICs, which were prepared at [PEG-PLL-SH]/[siRNA] = 1 in 10 mM Hepes buffer (pH 7.2), were mixed with 20 nm AuNPs at a molar ratio ([siRNA]/[AuNP]) = 360 in the same buffer, then incubated at 4 °C for 8 h. Unbound uPICs were removed thoroughly by repeated centrifugal steps and the resulting uPIC-AuNPs were dispersed in 10 mM Hepes buffer (pH 7.2) containing 150 mM NaCl. The successful conjugation of uPICs onto AuNP was verified by UV–vis absorbance spectra, transmission electron microscopy (TEM), and dynamic light scattering (DLS). The absorbance spectrum of uPIC-AuNPs suggested that flocculation of AuNPs hardly occurred during the conjugation process, as a notable change in the absorbance spectra based on the surface plasmon resonance was not observed between bare AuNPs and uPIC-AuNPs (Figure 3A). Furthermore, the TEM image depicted that the uPIC-AuNPs were composed of single AuNP without particle aggregation, as their spherical shapes with a narrow size distribution (Figure 3B) were similar to those of the bare AuNP templates (Figure S2 (SI)). On the other hand, the intensity-based DLS histograms clearly show an increase in size of AuNPs after uPIC conjugation (Figure 3C). The peak top in the histogram was shifted from *ca.* 23 nm in bare AuNPs to *ca.* 38 nm in uPIC-AuNPs. Considering that the siRNA length is *ca.* 6 nm[24] and a hydrodynamic radius of PEG (MW = 2200) in a random coil is *ca.* 1.5 nm,[25] this size increase is consistent with the conjugation of uPICs on AuNP, as illustrated in Figure 1B. In addition, the zeta-potential of uPIC-AuNPs was determined to be -24.7 ± 0.4 mV. This value was significantly higher in the positive direction than that of bare AuNPs (-31.3 ± 1.2 mV), consistent with the presence of PEG outer shell in uPIC-AuNPs. It should be noted that the uPIC-AuNPs maintained their

size and size distribution even after overnight incubation in 10% FBS-containing media (Figure 3C), indicating the high stability of these nanoarchitectures in the biological media. These results clearly demonstrate that the uPIC-AuNPs were successfully constructed in a size-regulated and monodispersed manner.

Next, the number of uPICs (or siRNAs) loaded in the uPIC-AuNPs was determined using a fluorescently labeled siRNA. The uPIC-AuNPs prepared with Alexa647-labeled siRNA (Alexa-siRNA) were treated with an excess amount of mercaptoethanol (12 mM) to induce a thiol exchange reaction on the AuNP surface.[19] The amount of released uPIC was quantified from its fluorescence intensity in the supernatant according to the standard curve (Figure S3 (SI)), and normalized by the amount of AuNP in solution. The number of loaded uPICs was calculated to be *ca.* 20 per AuNP. This value is slightly smaller than that for previous siRNA-loaded AuNP systems, where thiolated siRNAs were directly attached to AuNPs and the number of loaded siRNA amounted to *ca.* 30 per AuNP.[26] The difference between these two formulations could be explained by their different spacer length between thiol and the charged segment. The thiolated siRNA had a longer spacer than the present PEG-PLL-SH polymer, alleviating the steric repulsive effects on the AuNP surface.

With regard to the nanoconstruction of uPIC-AuNPs, it was verified whether the preformation of uPICs and the thiol moiety in PEG-PLL-SH were indispensable for successful preparation of the uPIC-AuNPs. When PEG-PLL-SH polymers were directly mixed with AuNPs prior to PIC formation (or in the absence of siRNA), visible flocculates were formed as indicated by the red-shift in their UV–vis absorbance spectrum (Figure 3A),[18] probably due to consecutive electrostatic binding between negatively charged citrate-stabilized AuNPs and oppositely charged PLL segments. On the other hand, the mixing between AuNPs and uPICs prepared with nonthiolated PEG-PLL led to the formation of considerably larger nanoparticles (DLS peak top: ~120 nm) with a broader size distribution (Figure 3C) and a slightly broader absorbance spectrum (Figure 3A) compared to the uPIC-AuNPs. This result indicates that a large number of AuNPs aggregated into larger particles under the physiological salt condition as a result of low colloidal stability through ineffective surface PEGylation in the absence of thiol-gold coordinate bonding. Note that bare AuNPs immediately aggregated to form visible flocculates by salting-out effect under the same condition (data not shown). Thus, the successful preparation of uPIC-AuNPs may stem from (i) the charge-neutralization of cationic PLL segment with siRNA, which reduces the electrostatic adsorptions between PLL chains and AuNPs, and (ii) the effective conjugation of uPICs (or PEG chains) onto AuNPs through thiol-gold coordinate bonding, which enhances colloidal stability.

The reversible stability of uPIC-AuNPs was verified by mimicking cytoplasmic reductive conditions as well as the extracellular conditions. The nanoarchitectures were incubated in a heparin solution with or without 10 mM GSH, which corresponds to the cytoplasmic concentration. In this stability assay, heparin was used as a representative of glycocalyx that is a major component of extracellular matrices and is abundant in the renal basement membrane. Glycocalyx is considered as a major obstacle for PIC-based siRNA delivery because PICs might be disrupted through electrostatic interactions with the negatively charged matrices.[27] In the absence of heparin and GSH, almost no bands derived from siRNA were observed for both uPICs and uPIC-AuNPs (Figure 4A), confirming the polyionic complexation of siRNA as indicated by the FCS result (Figure 2A). It should be noted that the staining of siRNA with SYBR Green II was significantly impaired when siRNA forms PICs with PEG-PLL, leading to almost no fluorescence signal from the siRNAs loaded by uPICs as well as uPIC-AuNPs. The heparin treatment induced a concentration-dependent siRNA release from uPICs and uPIC-AuNP by counter polyanion exchange. However, this release required more heparin in the case of uPIC-AuNPs compared to uPICs. In particular, while the released siRNA was clearly observed upon treatment of uPICs with 1 μg/mL of heparin, almost no band was detected for uPIC-AuNPs under the same conditions. These results indicate that uPICs conjugated onto the AuNP were more stable than free uPICs. This enhanced PIC stability may be attributed to the PEG outer layer surrounding uPIC-AuNP.

In contrast, the GSH-treated uPIC-AuNPs showed a band of released siRNA with smaller amount of heparin, compared to those in the absence of GSH, demonstrating the GSH-responsive siRNA release from uPIC-AuNPs. The underlying mechanism for this GSH-responsive release can be explained as follows. GSH (or its cystein thiol) can detach uPICs from AuNP through the thiol–thiol exchange reaction. The detached uPICs should become more sensitive for counter polyanion exchange with heparin as indicated by Figure 4A (uPIC + Heparin lanes *vs* uPIC-AuNP + Heparin lanes), resulting in the facilitated siRNA release. This can be explained by the fact that the cysteine thiol in GSH can competitively interact with coordinate bonds between uPICs and AuNP, forming alternative coordinate bonds with AuNPs (or uPICs) that promote the detachment of uPICs from uPIC-AuNPs. In this regard, it is worth mentioning that the GSH-treated uPIC-AuNPs also released siRNA in the absence of heparin. GSH alone did not release siRNA from uPICs even at 50 mM (Figure 4B), suggesting that the coexistence of GSH and AuNPs should be crucial for the siRNA release. We assumed that GSH-conjugated AuNPs (GSH-AuNPs), which should be generated by incubation of uPIC-AuNPs with GSH, might elicit siRNA release from

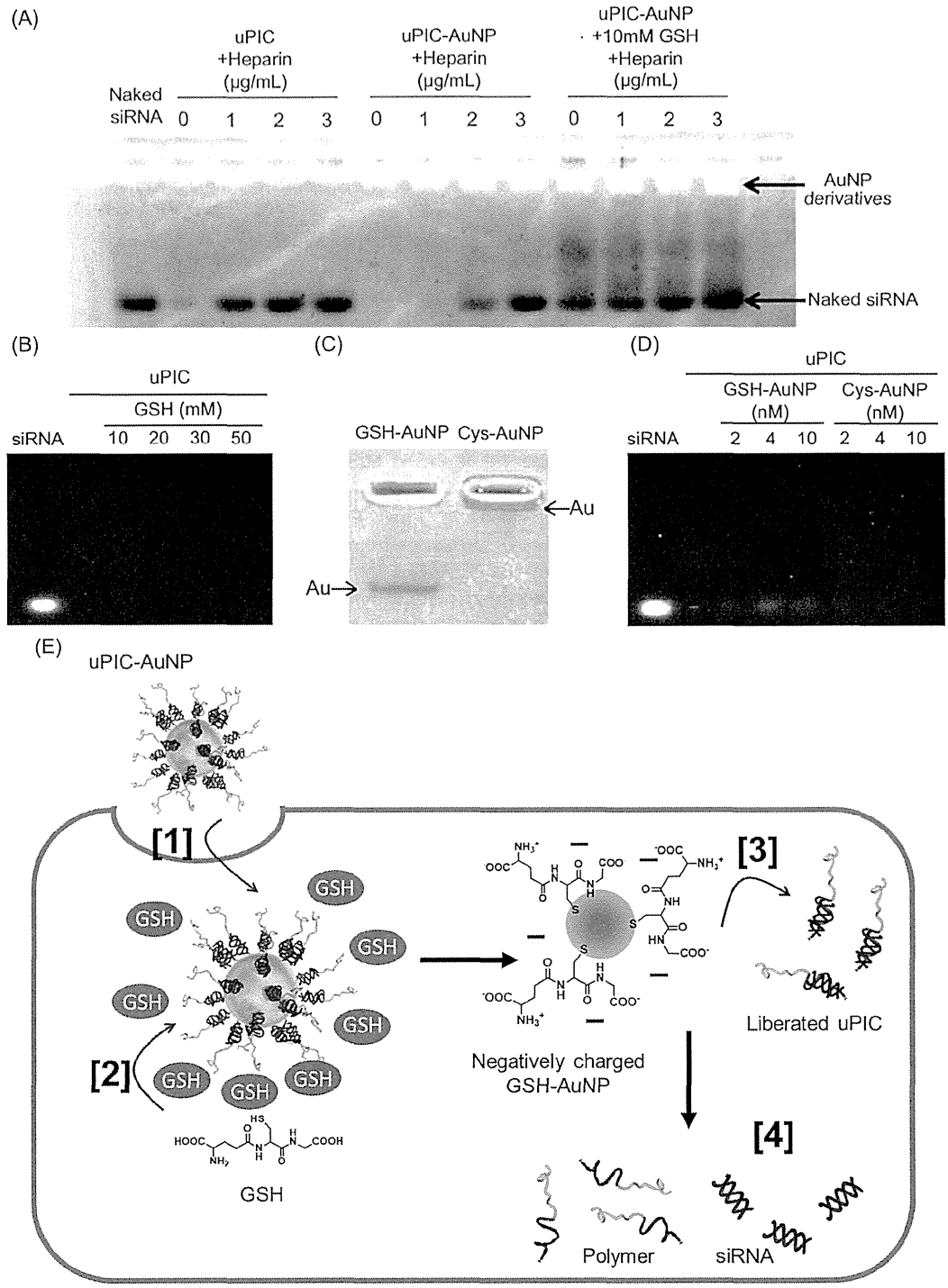

Figure 4. (A) Stability assay of uPICs and uPIC-AuNPs (400 nM siRNA) incubated with heparin (0, 1, 2, and 3 μg/mL) and GSH (0 and 10 mM). At 10 min after incubation, the solutions were loaded onto 1% agarose gel (1 × Tris/Borate/EDTA (TBE) buffer), subjected to a voltage of 100 V for 15 min, and stained with SYBR Green II. (B) Gel electrophoresis of uPICs solutions in the presence of various GSH concentrations. (C) Gel electrophoresis of AuNPs solutions treated with GSH or cysteine. Arrows indicate the AuNP positions. (D) Gel electrophoresis of uPICs solutions in the presence of AuNPs pretreated with GSH (GSH-AuNP) or with cysteine (Cys-AuNP). (E) Schematic illustration of the proposed mechanism for intracellular siRNA release from uPIC-AuNPs in the presence of GSH.

uPICs; the GSH-AuNPs that have negative surface charges derived from one excess of carboxyl group in GSH can bind to oppositely charged PEG-PLL in uPICs, directed toward siRNA release. To verify this assumption, an additional release assay was performed using GSH-AuNPs prepared as a negatively charged nanoparticle and cysteine-conjugated AuNPs (Cys-AuNPs) which were prepared as a control nanoparticle

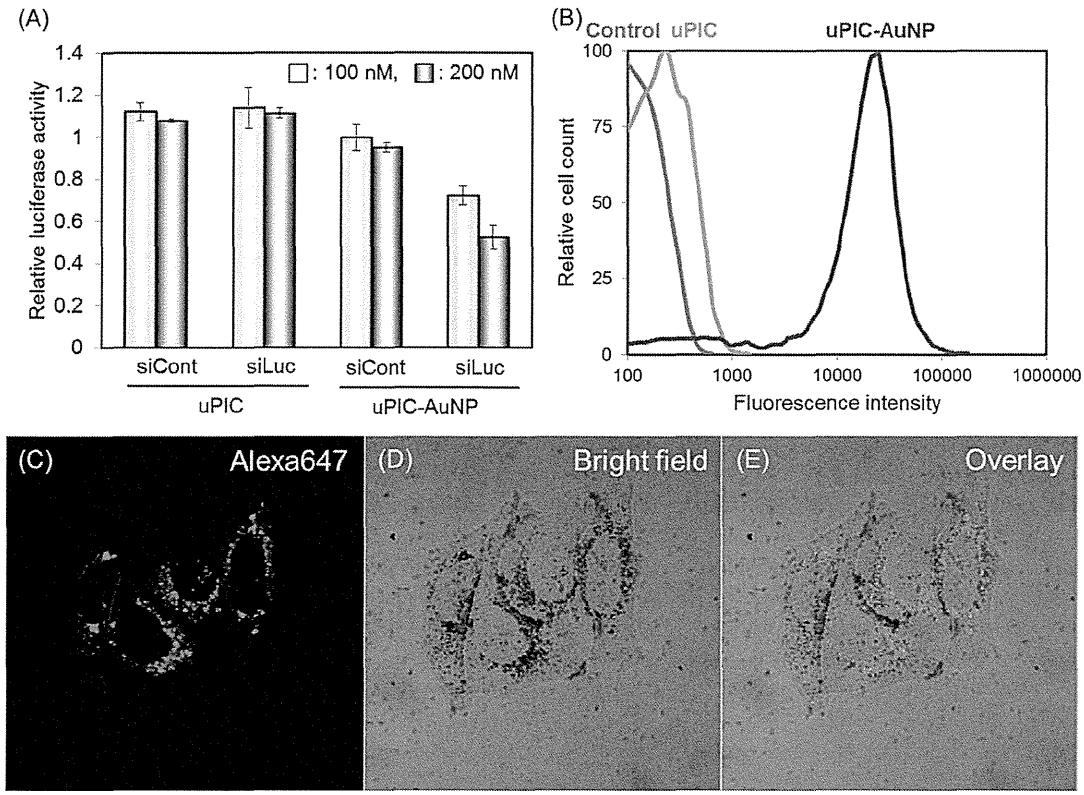

Figure 5. (A) Gene silencing efficiency of uPICs and uPIC-AuNPs loaded with siLuc or siCont at 100 and 200 nM siRNA in cultured HeLa-Luc cells after 48 h incubation. Results are expressed as mean and standard deviation (n = 4). (B) Flow cytometry analysis of siRNA cellular uptake efficiency in cultured HeLa-Luc cells incubated for 24 h with uPIC-AuNPs or uPICs at 200 nM Alexa-siRNA. (C–E) CLSM images of HeLa-Luc cells treated with uPIC-AuNPs at 200 nM Alexa-siRNA for 24 h.

modified with a neutral amino acid. The significant negative charges of GSH-AuNPs were confirmed by the agarose gel electrophoresis (Figure 4C), where GSH-AuNPs were clearly shifted to the positive electrode, compared to Cys-AuNPs. As expected, GSH-AuNPs permitted siRNA release from uPICs in a concentration-dependent manner (Figure 4D). In contrast, much lower amounts of released siRNA were detected using Cys-AuNPs (Figure 4D). These results are consistent with the above assumption that the negative charges derived from GSH conjugated on AuNPs should be crucial for the effective release of siRNA from uPICs. Altogether, it is strongly suggested that the uPIC-AuNPs internalized by cells should accelerate siRNA release in response to abundant cytoplasmic GSH, as illustrated in Figure 4E.

The stability of uPIC-AuNPs was further compared with a control conjugate without PEG-PLL (siRNA-AuNP), which was prepared by mixing thiolated siRNAs with AuNPs. In this stability assay, each conjugate prepared with Cy5-siRNA was incubated in 10 mM Hepes buffer (pH 7.2) containing 150 mM NaCl and 10% FBS. The fluorescence intensity derived from Cy5 was sequentially monitored using a plate reader, then normalized to that of free Cy5-siRNA (Figure S4 (SI)). The increase in the fluorescence intensity, presumably due to the dequenching effect of Cy5, was smaller in uPIC-AuNPs compared to siRNA-AuNPs, indicating that the uPIC-AuNPs more effectively suppressed disintegration of the conjugate structure (or degradation of siRNA) in the serum-containing medium. This result demonstrates an advantage of the conjugate formulation using PEG-PLL.

Cellular Delivery of siRNA with uPIC-AuNPs. Cellular delivery of siRNA by uPIC-AuNPs was first investigated by a luciferase assay, in which the gene silencing of uPIC-AuNPs was evaluated from the luciferase activity (or luminescence intensity) in cultured cervical cancer cells stably expressing luciferase (HeLa-Luc). Nanoarchitectures bearing luciferase siRNA (siLuc) or control siRNA (siCont) were incubated with HeLa-Luc cells for 48 h prior to the measurement of luminescence intensity. The uPIC-AuNPs carrying siLuc significantly reduced the luciferase activity, *i.e.*, ~25 and ~40% at 100 and 200 nM siRNA, respectively, whereas siCont-loaded controls showed no decrease in the luciferase activity (Figure 5A), demonstrating the sequence-specific gene silencing effect of uPIC-AuNPs. In sharp contrast, siLuc-loaded uPICs without AuNPs induced no gene silencing effect at both siRNA concentrations. These results indicate that the AuNPs templates were indispensable in enhancing the gene silencing effect

of uPIC-AuNPs. The gene silencing efficiency obtained by uPIC-AuNPs was apparently similar and lower compared to previously reported siRNA-conjugated AuNPs[26] and their complexes with cationic poly(β-amino ester)s,[28] respectively. The lower efficiency may be due to the PEG outer layer on uPIC-AuNP surface, which can compromise the adsorptive endocytosis of nanoparticles through the steric repulsive effect,[5] leading to less cellular uptake of siRNA compared to the positively charged nanoparticle carrier. Cell viability was further examined in cultured HeLa-Luc cells under the similar condition to the luciferase assay (Figure S5 (SI)). Neither uPIC-AuNPs nor uPICs affected the cell viability until 400 nM siRNA. Thus, negligible cytotoxic effect was confirmed for these formulations.

In order to elucidate which step in the cellular delivery of siRNA generated the dramatic improvement in the gene silencing effect of uPIC-AuNPs, we further addressed cellular uptake and intracellular trafficking studies using Alexa-siRNA. The cellular uptake efficiency of Alexa-siRNA was determined by flow cytometric analyses for the HeLa-Luc cells incubated with uPIC-AuNPs or uPICs at 200 nM Alexa-siRNA for 24 h (Figure 5B). Cells treated with uPIC-AuNPs exhibited 70-fold higher mean fluorescence intensity than those with uPICs without AuNPs, indicating a significantly enhanced cellular uptake of siRNA upon conjugation of uPIC to AuNPs. It should be further noted that the enhanced cellular uptake of uPIC-AuNPs was clearly observed even after treating the cells with a heparin/DTT solution after 6 and 24 h incubation (Figure S6 (SI)), suggesting that the Alexa-siRNA payloads should be within the cells but not bound to the cellular surface. This result matches the greater gene silencing effect of uPIC-AuNPs (Figure 5A). The higher efficiency of the cellular uptake of uPIC-AuNPs may be attributed to their higher stability against counter polyion exchange with negatively charged glycosaminoglycans, compared to uPICs (Figure 4A). uPIC-AuNPs should be more stable on the cell surface coated with anionic glycocalyx,[29] facilitating the cellular uptake of siRNA through charge-neutralization and reduced electrostatic repulsion between siRNA and the cell surface. The detailed mechanism for the cellular uptake of uPIC-AuNPs remains to be further investigated. The intracellular trafficking of uPIC-AuNPs was observed by a confocal laser scanning microscope (CLSM) (Figure 5C–E). While cells treated with uPICs exhibited almost no fluorescence (Figure S7 (SI)), the fluorescent signal of Alexa-siRNA was clearly observed in cells treated with uPIC-AuNPs (Figure 5C), consistent with flow cytometric results (Figure 5B). The bright field image depicts that numerous AuNPs were concurrently internalized by the cells and mainly distributed in the perinuclear region (Figure 5D). Based on the overlay image (Figure 5E), the correlation between intracellular Alexa-siRNA and AuNPs was then calculated to be nearly 1 by Mander's correlation coefficient. This high level of the correlation strongly suggests that siRNA molecules (or uPICs) are internalized together with AuNPs and subsequently delivered to the perinuclear regions, such as the late endosome or lysosome, by microtubule tracking.[30] Accordingly, siRNA translocation from the endosome or lysosome to the cytoplasm will be one of the critical steps for improving the gene silencing efficiency in a future study.

Systemic Delivery of siRNA to a Subcutaneous Tumor Model using uPIC-AuNPs. As demonstrated in many previous studies, sub-100 nm-sized nanoparticles featuring longevity in circulation can efficiently accumulate in solid tumors through the leaky tumor vasculature and immature lymphatic drainage *via* EPR effect.[11,12] The MW of uPICs was determined to be 22 000 Da by the AUC method, thereby they are expected to be eliminated by renal filtration.[31] Indeed, it was demonstrated that 90% of uPICs prepared with Alexa-siRNA were eliminated from the bloodstream in 10 min after intravenous injection (Figure S8 (SI)), when the fluorescence intensity from the vein of murine earlobe was time-dependently monitored by an intravital real-time confocal laser scanning microscope.[32,33] Thus, we conjugated uPICs onto AuNPs (20 nm in diameter) to regulate the carrier size for evading such rapid clearance, directed toward longer blood circulation. The uPIC-AuNPs (or bare AuNPs as a control) were injected intravenously into mice and blood samples were collected after a designated time. The concentration of AuNP in plasma was determined by ion coupled plasma-mass spectrometer (ICP-MS) and normalized to the initial dose. Note that the blood circulation time of uPIC-AuNPs was estimated by ICP-MS instead of confocal laser scanning microscope because the fluorescence intensity of Alexa-siRNA was considerably quenched on the AuNP surface. The time for 90% elimination of uPIC-AuNPs (*ca.* 180 min) was three times longer than that for bare AuNPs (*ca.* 60 min) (Figure 6A) and 1 order of magnitude longer than that for uPICs (*ca.* 10 min). The longer blood circulation time in uPIC-AuNP should be attributed to its uniformly controlled size at *ca.* 40 nm, circumventing renal filtration. This result also indicates that the uPICs conjugated on the AuNP significantly improved the blood circulation longevity of AuNPs, presumably because the PEG outer layer reduced nonspecific interactions with blood components.[5,34]

Next, the accumulation of systemically administered uPIC-AuNPs in subcutaneous HeLa-Luc tumors was evaluated based on the fluorescence intensity of excised tumors using an *in vivo* imaging system (IVIS) instrument and compared with several controls, such as naked siRNA, uPICs, and the mixture of AuNPs and uPICs without thiol (Figure 6B). The fluorescence intensities of Alexa-siRNA delivered by uPICs or the

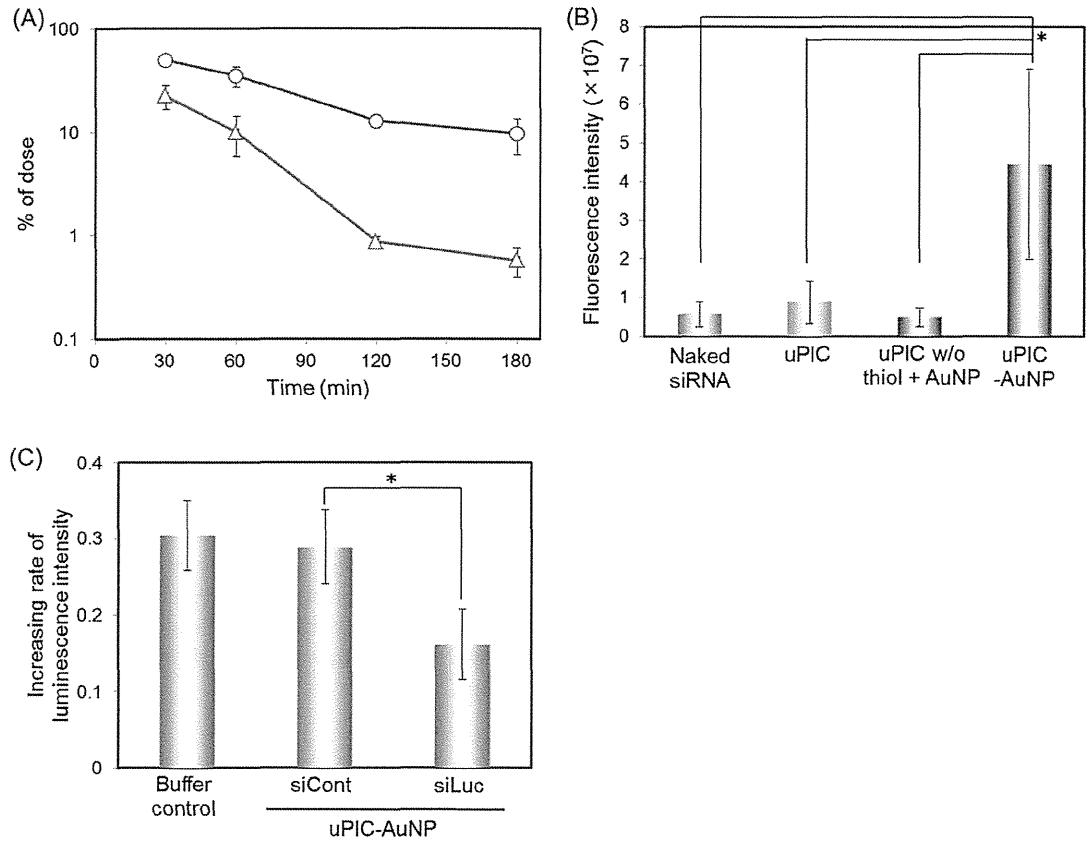

Figure 6. (A) Blood circulation property of uPIC-AuNPs (open circle) and bare AuNPs as a control (open triangle) determined by ICP-MS. Results are expressed as mean and standard deviation ($n = 3-4$). (B) Subcutaneous HeLa-Luc tumor accumulation of Alexa-siRNA delivered by each formulation at 4 h after intravenous injection (4.8 μg siRNA/mouse), determined by IVIS. Results are expressed as mean and standard deviation ($n = 4$, *: $P < 0.01$). (C) Increasing rate of luminescence intensity (IR_{LI}) from subcutaneous HeLa-Luc tumors after treatment with siLuc- or siCont-loaded uPIC-AuNPs (5.8 μg siRNA/mouse/shot) or a Hepes buffer control. The IR_{LI} values were calculated as an indicator of luciferase gene silencing activity, as described in the Materials and Methods. Results are expressed as mean and standard error of the mean ($n = 4$, *$P < 0.05$).

mixture of AuNP/uPICs without thiol were similar to that of naked Alexa-siRNA. In contrast, a significantly higher fluorescence intensity was observed for uPIC-AuNPs ($p < 0.01$ for the other samples), indicating the enhanced tumor accumulation of uPIC-AuNPs. This fluorescence intensity in the tumor was converted to 14 ± 4 in terms of % dose/g of tumor using a standard curve. Note that the fluorescence intensity of uPIC-AuNPs was likely to be underestimated compared to free uPICs because of the quenching effect of AuNPs: *ca.* 65% of the fluorescence signal was quenched in the uPIC-AuNPs. Apparently, this result is correlated with the blood circulation property of delivery carriers, as the efficient tumor accumulation was achieved by the long-circulating uPIC-AuNPs. Furthermore, the comparison between uPIC-AuNPs and the mixture of AuNP/uPICs without thiol reveals the key role of the strong binding between uPICs and AuNPs for the enhanced tumor accumulation of siRNA. Weakly bound uPICs on AuNPs might be readily detached from the nanotemplate in the circulation, presumably leading to the renal filtration, similar to uPICs without AuNPs and naked siRNA.

Finally, the gene silencing efficiency of systemically administered uPIC-AuNPs was investigated in subcutaneous HeLa-Luc tumors by the luciferase assay. The luminescence intensity emitted from HeLa-Luc tumors was measured using an IVIS instrument after intraperitoneal injection of a luciferin substrate. An increasing rate of luminescence intensity was significantly reduced to approximately 50% in the tumors treated with siLuc-containing uPIC-AuNPs, compared to a buffer-treated control and siCont-containing uPIC-AuNPs (Figure 6C). Thus, the uPIC-AuNPs were demonstrated to successfully induce the sequence-specific gene silencing in the tumor tissue through systemic administration, probably due to the efficient tumor accumulation associated with its longevity in the blood. It should be noted that severe cytokine induction was not observed after systemic administration of uPIC-AuNPs at the similar dose (Figure S10 (SI)). Interestingly, a slight increase in the TNF-α level observed for bare AuNPs at 6 h after injection was apparently reduced in uPIC-AuNPs, possibly due to the biologically inert PEGylated surface of uPIC-AuNPs.

Recent studies, including ours, revealed that precise size controlling below 100 nm had a great impact on the nanoparticle accumulation and permeation in a variety of tumor models. Specifically, sub-50 nm-sized nanoparticles achieved considerably higher accumulation efficiency in thick fibrotic pancreatic tumor tissues compared to 100 nm-sized controls.[13] The methodology developed in this study can build size-tunable nanoarchitectures featuring monodispersed uPIC building blocks and size-preset AuNP nanotemplates. Consequently, the constructed uPIC-AuNP nanoarchitectures enabled the efficient tumor accumulation of siRNA and significant *in vivo* gene silencing effect in the tumor, demonstrating their potential for siRNA-based cancer therapies.

CONCLUSIONS

In the present study, the size-tunable and reversibly stabilized nanoarchitecture was constructed with a monodispersed building block of uPICs and a size-preset nanotemplate of AuNPs for systemic siRNA delivery to solid tumors. The monodispersed uPICs were prepared with a single charged pair of siRNA and PEG-PLL-SH with the DP_{PLL} = ~40 based on the charge-matched polyionic complexation. Then, the uPICs were conjugated onto the AuNP having 20 nm size through the thiol-gold coordinate bonding. Successful construction of the nanoarchitecture uPIC-AuNPs was achieved by the preformation of uPICs and the stable bonding between uPICs and AuNP. The size of generated uPIC-AuNPs was precisely controlled in the range of less than 50 nm by the sizes of nanotemplate AuNP and surrounding uPICs. The uPIC-AuNPs efficiently delivered siRNA into cultured cancer cells, allowing the significant sequence-specific gene silencing without apparent cytotoxicity. The systemically administered uPIC-AuNPs showed much longer blood circulation property and significantly enhanced accumulation of siRNA in a subcutaneous cervical cancer model, compared to their component controls (bare AuNPs and uPICs). Ultimately, uPIC-AuNPs achieved the significant gene silencing in the tumor tissue through systemic administration. These results demonstrate the potential of uPIC-conjugated nanoarchitectures for systemic siRNA delivery toward RNAi-based cancer therapy.

MATERIALS AND METHODS

Materials. ε-Trifluoroacetyl-L-lysine *N*-carboxy anhydride (Lys(TFA)-NCA) was prepared by the Fuchs–Farthing method using triphosgene.[35] α-Methoxy-ω-amino PEG (PEG-NH_2, M_n = 2200) was obtained from NOF Co., Ltd. (Tokyo, Japan). *N,N*-Dimethylformamide (DMF) was purchased from Wako Pure Chemical Industries, Ltd. (Osaka, Japan). Dithiothreitol (DTT), dimethyl sulfoxide (DMSO), diisopropylethylamine (DIPEA), and Dulbecco's modified Eagle's media (DMEM) were purchased from Sigma-Aldrich Co. (St. Louis, MO, USA). DMSO, DMF, and DIPEA were purified by distillation under reduced pressure. Gold nanoparticle (20 nm in diameter) was purchased from BBInternational (Cardiff, UK). Succinimidyl 6-[3-(2-pyridyldithio)-propionamido]hexanoate (LC-SPDP) was obtained from Pierce (Rockford, IL, USA). Hepes (1 M, pH 7.3) was purchased from Amresco (Solon, OH, USA). The luciferase-expressing human cervical cancer cell line, HeLa-Luc, was purchased from Caliper LifeScience (Hopkinton, MA, USA). Fetal bovine serum was provided by Dainippon Sumitomo Pharma Co., Ltd. (Osaka, Japan). BALB/c nude and BALB/c mice were purchased from Charles River Japan (Kanagawa, Japan). siRNAs were synthesized by Hokkaido System Science Co., Ltd. (Hokkaido, Japan), and the sequences used are as follows: (1) Firefly GL3 luciferase (siLuc): 5′-CUU ACG CUG AGU ACU UCG AdTdT-3′ (*sense*), 5′-UCG AAG UAC UCA GCG UAA GdTdT-3′ (antisense); (2) control (siCont): 5′-UUC UCC GAA CGU GUC ACG UdTdT-3′ (sense), 5′-ACG UGA CAC GUU CGG AGA AdTdT-3′ (antisense). All dyes (Alexa647 and Cy3) were attached to 5′-end of sense stand of siLuc. All animal experiments were carried out in accordance with the guidelines for animal experiments at The University of Tokyo, Japan.

Synthesis of PEG-PLL(TFA). PEG-PLL(TFA) was prepared by ring-opening polymerization of Lys(TFA)-NCA, as previously described.[35] Briefly, Lys(TFA)-NCA (1 g, 3.7 mmol) was dissolved in DMSO (40 mL). After the addition of the macroinitiator PEG-NH_2 (176 mg, 88.8 μmol) to DMSO (7.0 mL), the reaction solution was stirred at 25 °C for 72 h under Ar. The resulting solution was precipitated into an excess amount of diethyl ether and dried *in vacuo*. The prepared PEG-PLL(TFA) was characterized by gel permeation chromatography (GPC) and ^{1}H NMR (400 MHz, ECS-400, JEOL, Tokyo, Japan). The DP of Lys(TFA) units was calculated to be 38 in the ^{1}H NMR spectrum from the peak intensity ratio of the β, γ, and δ-methylene protons of lysine ($-(CH_2)_3-$, $\delta \approx 1.4-1.8$) to the oxyethylene protons of PEG ($-(OCH_2CH_2)-$, δ = 3.7). The GPC system (HLC-8220, TOSOH CORPORATION, Tokyo, Japan) equipped with two TSK gel columns (TSK-gel Super AW4000 and Super AW3000) was eluted with DMF containing lithium chloride (10 mM) at 0.8 mL/min. Molecular weight distribution (M_w/M_n) of the block copolymer was determined to be 1.07.

Synthesis of PEG-PLL(TFA)-LC-SPDP. PEG-PLL(TFA) (46.5 mg, 4.47 μmol) was dissolved in DMF (2 mL) and stirred overnight at 40 °C under Ar. LC-SPDP (20.5 mg, 44.7 μmol) in DMF (1 mL) was added to the polymer solution and further stirred at 35 °C for 4 h. DIPEA (4 μL, 22.4 μmol) in DMF (0.4 mL) was added to the reacting solution and stirred overnight. The resulting solution was dialyzed against methanol and then deionized water, followed by lyophilization. The prepared PEG-PLL(TFA)-LC-SPDP was characterized in MeOD at 40 °C by ^{1}H NMR (400 MHz, ECS-400) from the peak intensity ratio of the methylene protons of dithiopropionyl group ($-COCH_2CH_2SS-$, δ = 2.3) to the oxyethylene protons of PEG ($-(OCH_2CH_2)-$, δ = 3.7). The conjugation ratio of LC-SPDP was calculated to be ~70%.

Deprotection of TFA and Pyridyl Groups. PEG-PLL(TFA)-LC-SPDP (20 mg) was dissolved in a mixed solvent of methanol (9 mL) and 1 N NaOH solution (1 mL), and then reacted at 35 °C for 8 h. The mixture was dialyzed against 0.01 N HCl and then deionized water. The final solution was lyophilized to obtain PEG-PLL-LC-SPDP in the chloride salt form. The deprotection of the TFA groups was confirmed in D_2O at 80 °C by ^{1}H NMR (400 MHz, ECS-400) from the peak shift of the ε-methylene protons from 3.0 to 3.3 ppm. For deprotection of pyridyl group, PEG-PLL-LC-SPDP (9 mg) was incubated with DTT (0.8 mg) at ambient temperature for 1 h in 10 mM sodium phosphate buffer (pH 7.2). The solution was dialyzed against 0.01 N HCl containing 1 mM EDTA for 2 h, 1 mM EDTA for 1 h, and then deionized water at 4 °C for 1 h. Finally, the product was lyophilized to obtain PEG-PLL-SH. Deprotection of pyridyl group was confirmed by Ellman's assay (data not shown).

Preparation of Single siRNA-Loaded uPICs and uPIC-installed Gold Nanoparticle (uPIC-AuNP). PEG-PLL-SH and siRNA were separately

dissolved in 10 mM Hepes buffer (pH 7.2) and mixed at varying molar ratios of PEG-PLL-SH to siRNA ([PEG-PLL-SH]/[siRNA]) to form uPICs (siRNA concentration: 17 μM). The uPIC solution was incubated for 1 h at ambient temperature. AuNP solution was concentrated to 60 nM by centrifugation (14 000 rpm, 10 min) in 20 μL and mixed with uPIC solution at a molar ratio of siRNA to AuNP ([siRNA]/[AuNP]) = 360. 10 mM Hepes buffer (pH 7.2) was added to the mixture for maintaining pH at 7.2, followed by 8 h incubation at 4 °C. Then, 2 M NaCl was added to the solution (final NaCl concentration: 150 mM). The solution was further incubated for 8 h. Unbound uPICs were removed by repeated centrifugations in 10 mM Hepes buffer (pH 7.2) containing 150 mM NaCl (14,000 rpm, 10 min). Finally, the uPIC-AuNPs were dispersed in 10 mM Hepes buffer (pH 7.2) containing 150 mM NaCl (AuNP concentration: 11 nM).

Diffusion Coefficient Measurements by Fluorescence Correlation Spectroscopy (FCS). FCS analyses were performed using a LSM510 confocal laser scanning microscope (CLSM, Carl Zeiss, Oberlochen, Germany) equipped with the Zeiss C-Apochromat 40× water objective and Confocor3 module. A He–Ne laser (543 nm) was used for Cy3-siRNA excitation and emission was obtained through a 560–615 nm band-pass filter. Samples were placed into 8-well Lab-Tek chambered borosilicate cover glass (Nalge Nunc International, Rochester, NY, USA) and measured at ambient temperature. The uPIC stability was evaluated in 10 mM Hepes buffer (pH 7.2) with or without 150 mM NaCl, as well as PBS containing 10% FBS. The uPICs prepared at 5 μM Cy3-siRNA were diluted with each media up to 10 nM Cy3-siRNA. After overnight incubation at 37 °C, the measurements were carried out with a sampling time of 10 s (10 measurements). The obtained autocorrelation curves were fitted with the Zeiss Confocor3 software package to calculate the diffusion coefficient.

Measurement of Molecular Weight (MW) of PICs by Analytical Ultracentrifuge (AUC). MW of PICs (MW_{PIC}) was determined by sedimentation equilibrium experiments with AUC equipped with absorbance optics (Beckman Coulter, CA, USA). The PIC solution was diluted up to 0.6 μM siRNA concentration with 10 mM Hepes buffer (pH 7.2) containing 150 mM NaCl. Absorbance at 260 nm was measured as a function of centrifugal radius (r) at 20 °C, and the obtained data was analyzed by ORIGIN software (Beckman Coulter, CA, USA) to determine the MW_{PIC} by the following equation based on the values of partial specific volume of PICs (PSV_{PIC}) and the buffer density.

$$\ln(C(r)/C(r_0)) = MW_{PIC} \times (1 - PSV_{PIC} \times \rho_0) \times \omega^2 \times (r^2 - r_0^2)/2RT$$

where $C(r)$ is a concentration of siRNA at r, ω is rotational speed, R is the gas constant, T is the temperature, and $C(r_0)$ is a concentration of siRNA at a reference radial distance. PSV_{PIC} was determined as a mass average of PSV_{siRNA} and $PSV_{PEG\text{-}PLL}$.

$$PSV_{PIC} = (M_{PEG\text{-}PLL} \times PSV_{PEG\text{-}PLL} + M_{siRNA} \times PSV_{siRNA})/(M_{PEG\text{-}PLL} + M_{siRNA})$$

where $M_{PEG\text{-}PLL}$ and M_{siRNA} are the mass of PEG-PLL and siRNA, respectively, in the solution. Each value was calculated from the density of siRNA or PEG-PLL solution measured by a density meter DMA4500/DMA5000 (Anton Paar, Graz, Austria). All the siRNA and PEG-PLL solutions were diluted up to 1, 2, and 5 mg/mL with 10 mM Hepes buffer (pH 7.2) containing 150 mM NaCl, and then the density measurements were performed at 20 °C. The PSV of component i (PSV_i) was calculated from the following equation:

$$PSV_i = (1 - d\rho/dc)/\rho_0$$

where ρ_0 is the density of buffer, ρ is the density of solution, and c is the concentration of solute. From the experiments, PSV_{PIC} and MW_{PIC} were determined to be 0.602 cm^3/g and 22 000 g/mol, respectively.

Physicochemical Characterizations of uPIC-AuNPs. UV–vis absorbance spectra of uPIC-AuNPs and the other control samples at 12 nM AuNP were measured using NanoDrop (Thermo Fisher Scientific Inc., Waltham, MA, USA). Sample sizes were determined at 25 °C by dynamic light scattering (DLS) method using a Zetasizer (Malvern Instruments Ltd., Worcestershire, UK) equipped with a He–Ne laser (λ = 633 nm) as the incident beam at a detection angle of 173°. The data obtained from the rate of decay in the photon correlation function were analyzed by the histogram method. Zeta-potentials of samples were also determined using the same apparatus.

Transmission Electron Microscopy (TEM) Observation. The morphologies of AuNPs and uPIC-AuNPs were examined using a TEM (JEM-1400, JEOL, Tokyo, Japan) at an acceleration voltage of 100 kV and a beam current of 40 μA. Each sample was stained with uranyl acetate solution (2 w/v%) and placed on 400-mesh copper grids.

Gel Electrophoresis. uPIC or uPIC-AuNP solution was mixed with heparin and GSH, and the mixtures were incubated for 10 min at room temperature (siRNA: 400 nM, heparin: 0, 1, 2, and 3 μg/mL, GSH: 0 and 10 mM). Then, the mixtures were analyzed by gel electrophoresis (1% agarose, 1 × TBE buffer, 100 V, 15 min). After staining with SYBR Green II, the band from siRNA was detected using a Molecular Imager FX (BIO-RAD) (Ex/Em: 488/530 nm) equipped with Quantity One software (BIO-RAD). In the other experiments, (i) uPIC solutions were incubated with GSH for 15 min at room temperature (GSH concentrations; 0, 10, 20, 30, and 50 mM), (ii) AuNP solutions were treated with 10 mM GSH or 10 mM cysteine for 10 min at room temperature, and then mixed with uPIC solutions, followed by additional incubation for 10 min (siRNA: 400 nM, AuNP: 0, 2, 4, and 10 nM), and (iii) AuNPs were treated with 10 mM cysteine or 10 mM GSH for 10 min at room temperature (AuNP: 4 nM).

***In Vitro* Luciferase Assay.** HeLa-Luc cells were seeded on a 96-well plate at a density of 5000 cells/well in DMEM containing 10% FBS (DMEM/FBS). siLuc or siCont-loaded uPIC-AuNPs were added to the cells and incubated for 48 h. Next, the cells were lysed using the cell lysis buffer (Promega, Fitchburg, WI, USA). Luminescence intensities of cell lysates were measured using the Luciferase Assay System (Promega) on a luminescence microplate reader (Mithras LB 940, Berthold technologies, Bad Wildbad, Germany). The relative luciferase activity was determined by normalizing the luminescence intensity of the sample-treated lysates to the amount of proteins contained in the lysates (determined using a BCA assay kit), followed by further normalization to buffer-treated controls (n = 4).

Flow Cytometric Analysis. HeLa-Luc cells were seeded on a 6-well plate at a density of 100 000 cells/well in DMEM/FBS. uPIC-AuNPs or uPICs prepared with Alexa647-labeled siRNA were added to the cells at 200 nM siRNA. After 24 h incubation, the media was removed and the cells were washed with cold PBS twice. The cells were treated with a trypsin-EDTA solution for 2 min and then suspended in cold PBS. The fluorescence intensity of Alexa647-labeled siRNA from the cells was measured using a BD LSR II (BD Biosciences, San Jose, CA, USA). The cells treated with 10 mM Hepes buffer (pH 7.2) containing 150 mM NaCl were used as a control.

Confocal Laser Scanning Microscopic (CLSM) Observation. HeLa-Luc cells were seeded on a 35 mm glass-based dish (Iwaki, Tokyo, Japan) at a density of 50 000 cells/well in DMEM/FBS. The uPIC-AuNPs loading Alexa647-labeled siRNA were added to the cells at 200 nM siRNA. After 24 h incubation, the culture media was removed and the cells were washed with cold PBS twice. Each dish was observed using a CLSM (LSM 510, Carl Zeiss) equipped with a Zeiss C-Apochromat 63× objective (Carl Zeiss). The excitation wavelength was set at 633 nm (He–Ne laser) for Alexa647-labeled siRNA, and the emission was detected between 651 and 704 nm.

Quantification of Blood Circulation of uPIC-AuNPs. siCont-loaded uPIC-AuNPs were intravenously injected (AuNP: 3.3 × 10^{12} particles/mouse, siRNA: 1.4 μg/mouse) into the tail vein of mice (BALB/c, female, 8 week old). The mice were sacrificed at a designated time and the collected blood was centrifuged (1500 rpm, 3 min) to obtain the plasma (20 μL). The plasma was treated with 90% HNO_3 by heating and stored in 1% HNO_3 solution overnight. The resulting sample solution was filtered using a 0.45 μm pore size membrane filter and further diluted to a desired concentration using 1% HNO_3 solution. The Au content was determined by ICP-MS (7700 Series, Agilent Technologies, Santa Clara, CA, USA).

Accumulation of uPIC-AuNPs in a Subcutaneous HeLa-Luc Tumor. Tumor accumulation of uPIC-AuNPs was determined in mice bearing a subcutaneous HeLa-Luc tumor. Tumors were prepared by injecting 5×10^6 cells under the skin in the left rear flank of mice (BALB/c nude, female, 8 week old), and were allowed to mature for 2 weeks ($n = 4$). Mice were fed with an alfalfa-free chow for 2 weeks before sample injection. uPIC-AuNPs or the other control samples (naked siRNA, uPICs, and the mixture of uPICs without thiol and AuNPs) prepared with Alexa647-labeled siRNA were injected into the tail vein of mice (4.8 μg siRNA/mouse). After 4 h, mice were sacrificed and tumor was excised. The excised tumor was imaged using an IVIS instrument (Caliper LifeScience, Hopkinton, MA, USA) in the fluorescence mode with appropriate filters for excitation (640 nm) and emission (720 nm). Data were analyzed using Living Image software (Caliper LifeScience) by drawing ROIs around the tumor to determine the fluorescence intensity and normalized with the background signal from nontreated tumors. Accumulation of siRNA in the tumor was expressed as an average of fluorescence intensity/tumor area.

***In Vivo* Luciferase Assay in Subcutaneous HeLa-Luc Tumor.** *In vivo* luciferase gene silencing ability was determined for mice bearing subcutaneous HeLa-Luc tumors, following the scheme shown in Figure S9A (SI). Tumors were prepared by injecting 5×10^6 cells under the skin in the right rear flank of mice (BALB/c nude, female, 8 week old) at day 0. The uPIC-AuNPs containing siLuc or siCont were intravenously injected into the tail vein of mice at days 17 and 18 (5.8 μg siRNA/mouse/shot). The luminescence intensity (lI) from the tumors was measured at days 17, 18, and 19 by an IVIS instrument equipped with a Living Image software (PerkinElmer). The luciferase gene silencing ability of uPIC-AuNPs was estimated from an increasing rate of LI (IR_{LI}) associated with the tumor growth. By assuming that the LI from the tumor should be proportional to the tumor volume (or the number of cancer cells), the IR_{LI} can be expressed as $\ln(LI_{t+1}/LI_t)$, where LI_t is the luminescence intensity from the tumor at day t, according to the calculating formula of the growth rate of tumor (GR): $GR = \ln(V_{t+1}/V_t)$, where V_t is the tumor volume at day t.[36] The IR_{LI} values between days 17 and 18 (after first injection), and days 18 and 19 (after second injection) were calculated using the LI measured at each day (Figure S9B (SI)), and further averaged to estimate the overall IR_{LI}, *i.e.*, $[\ln(LI_{18}/LI_{17}) + \ln(LI_{19}/LI_{18})]/2$, as an indicator of luciferase gene silencing activity (Figure 6C).

Conflict of Interest: The authors declare no competing financial interest.

Acknowledgment. This research was financially supported by the Funding Program for World-Leading Innovative R&D in Science and Technology (FIRST) (JSPS), Grants-in-Aid for Scientific Research of MEXT (JSPS KAKENHI Grant Numbers 25000006 and 25282141), the Center of Innovation (COI) Program (JST), Grants-in-Aid for Scientific Research of MHLW, and National Institute of Biomedical Innovation. H. J. Kim would like to thank A. Kim for his help with the TEM imaging of gold nanoparticles and also S. Chuanoi for his assistance with polymer synthesis.

Supporting Information Available: ^{1}H NMR of PEG-PLL-SH, TEM image of bare AuNPs, fluorescence intensity plotted against various uPIC concentrations, viability of HeLa-Luc cells treated with uPIC-AuNPs or uPICs, CLSM images of HeLa-Luc cells treated with uPICs. This material is available free of charge *via* the Internet at http://pubs.acs.org.

REFERENCES AND NOTES

1. Aagaard, L.; Rossi, J. J. RNAi Therapeutics: Principles, Prospects and Challenges. *Adv. Drug Delivery Rev.* **2007**, *59*, 75–86.
2. Burnett, J. C.; Rossi, J. J. RNA-Based Therapeutics: Current Progress and Future Prospects. *Chem. Biol.* **2012**, *19*, 60–71.
3. Dykxhoorn, D. M. RNA Interferences as an Anticancer Therapy: a Patent Perspective. *Expert Opin. Ther. Pat.* **2009**, *19*, 475–491.
4. He, S.; Zhang, D.; Cheng, F.; Gong, F.; Guo, Y. Applications of RNA Interference in Cancer Therapeutics as a Powerful Tool for Suppressing Gene Expression. *Mol. Biol. Rep.* **2009**, *36*, 2153–2163.
5. Nishiyama, N.; Kataoka, K. Current State, Achievements, and Future Prospects of Polymeric Micelles as Nanocarriers for Drug and Gene Delivery. *Pharmacol. Ther.* **2006**, *112*, 630–648.
6. Lee, Y.; Kataoka, K. Biosignal-Sensitive Polyion Complex Micelles for the Delivery of Biopharmaceuticals. *Soft Matter* **2009**, *5*, 3810–3817.
7. Guo, X.; Huang, L. Recent Advances in Nonviral Vectors for Gene Delivery. *Acc. Chem. Res.* **2012**, *45*, 971–979.
8. Wagner, E. Polymers for siRNA Delivery: Inspired by Viruses to be Targeted, Dynamic, and Precise. *Acc. Chem. Res.* **2012**, *45*, 1005–1013.
9. Nakase, I.; Akita, H.; Kogure, K.; Graslund, A.; Langel, U.; Harashima, H.; Futaki, S. Efficient Intracellular Delivery of Nucleic Acid Pharmaceuticals Using Cell-Penetrating Peptides. *Acc. Chem. Res.* **2012**, *45*, 1132–1139.
10. Kanasty, R. L.; Whitehead, K. A.; Vegas, A. J.; Anderson, D. G. Action and Reaction: the Biological Response to siRNA and Its Delivery Vehicles. *Mol. Ther.* **2012**, *20*, 513–524.
11. Matsumura, Y.; Maeda, H. A New Concept for Macromolecular Therapeutics in Cancer Chemotherapy: Mechanism of Tumoritropic Accumulation of Proteins and the Antitumor Agent Smancs. *Cancer Res.* **1986**, *46*, 6387–6392.
12. Maeda, H. Macromolecular Therapeutics in Cancer Treatment: the EPR Effect and Beyond. *J. Controlled Release* **2012**, *164*, 138–144.
13. Cabral, H.; Matsumoto, Y.; Mizuno, K.; Chen, Q.; Murakami, M.; Kimura, M.; Terada, Y.; Kano, M. R.; Miyazono, K.; Uesaka, M.; *et al.* Accumulation of Sub-100 nm Polymeric Micelles in Poorly Permeable Tumors Depends on Size. *Nat. Nanotechnol.* **2011**, *6*, 815–823.
14. Tang, L.; Fan, T. M.; Borst, L. B.; Cheng, J. Synthesis and Biological Response of Size-Specific, Monodisperse Drug-Silica Nanoconjugates. *ACS Nano* **2012**, *6*, 3954–3966.
15. Harada, A.; Kataoka, K. Chain Length Recognition: Core-Shell Supramolecular Assembly from Oppositely Charged Block Copolymers. *Science* **1999**, *283*, 65–67.
16. DeRouchey, J.; Schmidt, C.; Walker, G. F.; Koch, C.; Plank, C.; Wagner, E.; Radler, J. O. Monomolecular Assembly of siRNA and Poly(ethylene glycol)-Peptide Copolymers. *Biomacromolecules* **2008**, *9*, 724–732.
17. Shimizu, H.; Hori, Y.; Kaname, S.; Yamada, K.; Nishiyama, N.; Matsumoto, S.; Miyata, K.; Oba, M.; Yamada, A.; Kataoka, K.; *et al.* siRNA-Based Therapy Ameliorates Glomerulonephritis. *J. Am. Soc. Nephrol.* **2010**, *21*, 622–633.
18. Rosi, N. L.; Mirkin, C. A. Nanostructures in Biodiagnostics. *Chem. Rev.* **2005**, *105*, 1547–1562.
19. Nel, A. E.; Madler, L.; Velegol, D.; Xia, T.; Hoek, E. M. V.; Somasundaran, P.; Klaessig, F.; Castranova, V.; Thompson, M. Understanding Biophysicochemical Interactions at the Nano-Bio Interface. *Nat. Mater.* **2009**, *8*, 543–557.
20. Saito, G.; Swanson, J. A.; Lee, K.-D. Drug Delivery Strategy Utilizing Conjugation *via* Reversible Disulfide Linkages: Role and Site of Cellular Reducing Activities. *Adv. Drug Delivery Rev.* **2003**, *55*, 199–215.
21. Buyens, K.; Meyer, M.; Wagner, E.; Demeester, J.; De Smedt, S. C.; Sanders, N. N. Monitoring the Disassembly of siRNA Polyplexes in Serum is Crucial for Predicting Their Biological Efficacy. *J. Controlled Release* **2010**, *141*, 38–41.
22. Kim, H. J.; Ishii, A.; Miyata, K.; Lee, Y.; Wu, S.; Oba, M.; Nishiyama, N.; Kataoka, K. Introduction of Stearoyl Moieties into a Biocompatible Cationic Polyaspartamide Derivative, PAsp(DET), with Endosomal Escaping Function for Enhanced siRNA-Mediated Gene Knockdown. *J. Controlled Release* **2010**, *145*, 141–148.
23. Rana, T. M. Illuminating the Silence: Understanding the Structure and Function of Small RNAs. *Nat. Rev. Mol. Cell Biol.* **2007**, *8*, 23–36.
24. Abels, J. A.; Moresno-Herrero, F.; Van der Heijden, T.; Dekker, C.; Dekker, N. H. Single-Molecule Measurements

of the Persistence Length of Double-Stranded RNA. *Biophys. J.* **2005**, *88*, 2737–2744.
25. Kenausis, G. L.; Voros, J.; Elbert, D. L.; Huang, N.; Hofer, R.; Ruiz-Taylor, L.; Textor, M.; Hubbell, J. A.; Spencer, N. D. Poly(L-lysine)-g-Poly(ethylene glycol) Layers on Metal Oxide Surfaces: Attachment Mechanism and Effects of Polymer Architecture on Resistance to Protein Adsorption. *J. Phys. Chem. B* **2000**, *104*, 3298–3309.
26. Giljohann, D. A.; Seferos, D. S.; Prigodich, A. E.; Patel, P. C.; Mirkin, C. A. Gene Regulation with Polyvalent siRNA-Nanoparticle Conjugates. *J. Am. Chem. Soc.* **2009**, *131*, 2072–2073.
27. Zuckerman, J. E.; Choi, C. H. J.; Han, H.; Davis, M. E.; Polycation-siRNA Nanoparticles, Can Disassemble at the Kidney Glomerular Basement Membrane. *Proc. Natl. Acad. Sci. U. S. A.* **2012**, *109*, 3137–3142.
28. Lee, J.-S.; Green, J. J.; Love, K. T.; Sunshine, J.; Langer, R.; Anderson, D. G. Gold, Poly(β-amino ester) Nanoparticles for Small Interfering RNA Delivery. *Nano Lett.* **2009**, *9*, 2403–2406.
29. Mislick, K. A.; Baldeschwieler, J. D. Evidence for the Role of Proteoglycans in Cation-Mediated Gene Transfer. *Proc. Natl. Acad. Sci. U. S. A.* **1996**, *93*, 12349–12354.
30. Chithrani, D. B. Intracellular Uptake, Transport, and Processing of Gold Nanostructures. *Mol. Membr. Biol.* **2010**, *27*, 299–311.
31. Seymour, L. W.; Duncan, R.; Strohalm, J.; Kopecek, J. Effect of Molecular Weight (Mw) of *N*-(2-Hydroxypropyl)-methacrylamide Copolymers on Body Distribution and Rate of Excretion After Subcutaneous, Intraperitoneal, and Intravenous Administration to Rats. *J. Biomed. Mater. Res.* **1987**, *21*, 1341–1358.
32. Matsumoto, Y.; Nomoto, T.; Cabral, H.; Matsumoto, Y.; Watanabe, S.; Christie, R. J.; Miyata, K.; Oba, M.; Ogura, T.; Yamasaki, Y.; *et al.* Direct and Instantaneous Observation of Intravenously Injected Substances Using Intravital Confocal Micro-Videography. *Biomed. Opt. Express* **2010**, *1*, 1209–1216.
33. Kim, H. J.; Oba, M.; Pittella, F.; Nomoto, T.; Cabral, H.; Matsumoto, Y.; Miyata, K.; Nishiyama, N.; Kataoka, K. PEG-Detachable Cationic Polyaspartamide Derivatives Bearing Stearoyl Moieties for Systemic siRNA Delivery toward Subcutaneous BxPC3 Pancreatic Tumor. *J. Drug Targeting* **2012**, *20*, 33–42.
34. Nomoto, T.; Matsumoto, Y.; Miyata, K.; Oba, M.; Fukushima, S.; Nishiyama, N.; Yamasoba, T.; Kataoka, K. *In Situ* Quantitative Monitoring of Polyplexes and Polyplex Micelles in the Blood Circulation Using Intravital Real-Time Confocal Laser Scanning Microscopy. *J. Controlled Release* **2011**, *151*, 104–109.
35. Harada, A.; Kataoka, K. Formation of Polyion Complex Micelles in an Aqueous Milieu from a Pair of Oppositely-Charged Block Copolymers with Poly(ethylene glycol) Segments. *Macromolecules* **1995**, *28*, 5294–5299.
36. Mehrara, E.; Forssell-Aronsson, E.; Ahlman, H.; Bernhardt, P. Quantitative Analysis of Tumor Growth Rate and Changes in Tumor Marker Level: Specific Growth Rate *Versus* Doubling Time. *Acta Oncol.* **2009**, *48*, 591–597.

JACS
JOURNAL OF THE AMERICAN CHEMICAL SOCIETY

Article

pubs.acs.org/JACS

Terms of Use

Modulated Protonation of Side Chain Aminoethylene Repeats in N-Substituted Polyaspartamides Promotes mRNA Transfection

Hirokuni Uchida,[†] Keiji Itaka,[†] Takahiro Nomoto,[‡] Takehiko Ishii,[‡] Tomoya Suma,[∥] Masaru Ikegami,[†] Kanjiro Miyata,[†] Makoto Oba,[⊥] Nobuhiro Nishiyama,[#] and Kazunori Kataoka*[,†,‡,§]

[†]Center for Disease Biology and Integrative Medicine, Graduate School of Medicine, [‡]Department of Bioengineering, Graduate School of Engineering, and [§]Department of Materials Engineering, Graduate School of Engineering, The University of Tokyo, 7-3-1 Hongo, Bunkyo, Tokyo 113-8656, Japan

[∥]Department of Chemical and Biomolecular Engineering, The University of Melbourne, Victoria 3010, Australia

[⊥]Graduate School of Biomedical Sciences, Nagasaki University, 1-14 Bunkyo-machi, Nagasaki 852-8521, Japan

[#]Polymer Chemistry Division, Chemical Resources Laboratory, Tokyo Institute of Technology, R1-11, 4529 Nagatsuta, Midori-ku, Yokohama 226-8503, Japan

S *Supporting Information*

ABSTRACT: Fine-tuning of chemical structures of polycation-based carriers (polyplexes) is an attractive strategy for safe and efficient mRNA transfaction. Here, mRNA polyplexes comprising N-substituted polyaspartamides with varied numbers of side chain aminoethylene repeats were constructed, and their transfection ability against human hepatoma cells was examined. Transfection efficacy clearly correlated with the number of aminoethylene repeats: polyplexes with odd number repeats (PA-Os) produced sustained increases in mRNA expression compared with those with even number repeats (PA-Es). This predominant efficacy of PA-Os over PA-Es was contradictory to our previous findings for pDNA polyplexes prepared from the same N-substituted polyaspartamides, that is, PA-Es revealed superior transfection efficacy of pDNA than PA-Os. Intracellular FRET analysis using flow cytometry and polyplex tracking under confocal laser scanning microscopy revealed that overall transfection efficacy was determined through the balance between endosomal escaping capability and stability of translocated mRNA in cytoplasm. PA-Es efficiently transported mRNA into the cytoplasm. However, their poor cytoplasmic stability led to facile degradation of mRNA, resulting in a less durable pattern of transfection. Alternatively, PA-Os with limited capability of endosomal escape eventually protect mRNA in the cytoplasm to induce sustainable mRNA expression. Higher cytoplasmic stability of pDNA compared to mRNA may shift the limiting step in transfection from cytoplasmic stability to endosomal escape capacity, thereby giving an opposite odd–even effect in transfection efficacy. Endosomal escaping capability and nuclease stability of polyplexes are correlated with the modulated protonation behavior in aminoethylene repeats responding to pH, appealing the substantial importance of chemistry to design polycation structures for promoted mRNA transfection.

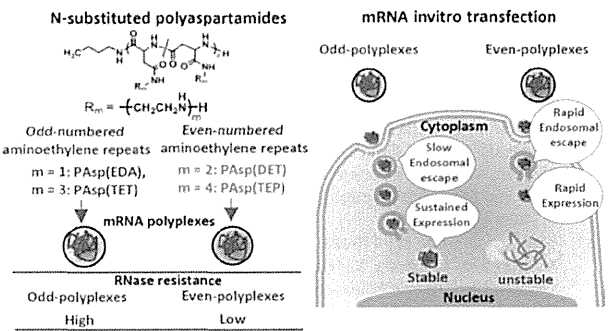

INTRODUCTION

Messenger RNA (mRNA) has attracted attention as a novel nucleic acid medicine for gene regulation therapy.[1,2] However, wide application has been limited because of the extremely labile nature of mRNA under physiological conditions, which hamper efficient and sustained delivery of mRNA. Polycations have been extensively studied for the delivery of nucleic acids because of their electrostatic interactions with nucleic acids, allowing the complex formation, which were termed "polyplex".[3−6] Polyplex systems can enhance cellular uptake and protect nucleic acids from nuclease digestion. Therefore, this system is considered to have high feasibility for effective delivery of mRNA, although few studies have focused on the chemical design of polycations customized for mRNA delivery.

Fine-tuning of chemical structures of polycations could dramatically improve the capability of polyplexes to overcome several barriers for successful polyplex transfection.[7−11] One of the critical barriers of polyplex transfection is inefficient translocation from endosomes into cytoplasm.[12] In our previous study directing to develop plasmid DNA (pDNA)-loaded polyplexes, the systematically varied number of aminoethylene repeats in the side chain on N-substituteted polyaspartamides revealed a marked impact on transfection efficiency of pDNA polyplexes. The polycations with an even number of aminoethylene repeats gave rise to polyplexes with

Received: June 20, 2014
Published: August 18, 2014

substantially higher transfection efficacy than those with an odd number of repeats.[9] This odd–even effect correlated with endosomal escape of polyplexes, which was greater for polyplexes with an even number of aminoethylene repeats. These observations can be ascribed to its potential to undergo an abrupt increase in the protonation degree of the side chain aminoethylene repeats in response to a decrease in the pH from physiological condition (~7.4) to acidic condition (~5.5), which corresponds to endosomal compartment.

This odd–even effect of N-substituted polyaspartamides was expected to remain intact during application for delivery of mRNA. Unprecedentedly, mRNA polyplexes with an odd number of aminoethylene repeats revealed much more durable and higher transfection efficacy than those with an even number of repeats. These unique findings are apparently contradictory to pDNA results, motivating us to carry out the present study to clarify the key structural parameters that determine the transfection efficacy of mRNA polyplexes formed using these polycations. The present data demonstrate the importance of fine-tuning in chemistry to regulate each key step that is involved in mRNA transfection toward the maximized efficacy.

EXPERIMENTAL SECTION

Materials. β-Benzyl-L-aspartate *N*-carboxyanhydride (BLA-NCA) was purchased from Chuo Kasei Co. Ltd. (Osaka, Japan). *N*-Methyl-2-pyrrolidone (NMP) was purchased from Nakalai Tesque Inc. (Kyoto, Japan). *N*,*N*-Dimethylformamide (DMF), dichloromethane (CH_2Cl_2), *n*-butylamine, ethylenediamine (EDA), diethylenetriamine (DET), triethylenetetramine (TET), tetraethylenepentamine (TEP), tris-(hydroxymethyl)aminomethane (Tris), 2-[4-(2-hydroxyethyl)-1-piperazinyl]ethanesulfonic acid (HEPES), and 2-morpholinoethanesulfonic acid monohydrate (MES) were purchased from Wako Pure Chemical Industries, Ltd. (Osaka, Japan). NMP, DMF, CH_2Cl_2, EDA, DET, TET, and TEP were used after conventional distillation. Dulbecco's modified Eagle's medium (DMEM) was purchased from Sigma-Aldrich Co. (St. Louis, MO). A plasmid DNA (pDNA) encoding Gaussia luciferase (GLuc) was purchased from New England BioLabs (Ipswich, CA). NucleoBond Xtra Maxi Plus for purification of competent DH5α *Escherichia coli* was purchased from Clontech Laboratories, Inc. (Mountain View, CA). Label IT Cy3 Labeling Kit and Label IT Cy5 Labeling Kit were purchased from Mirus Bio Corporation (Madison, WI). The transfection reagent ExGen 500 (linear polyethylenimine) was purchased from Fermentas LLC (Harrington Court, Canada). 96-Well and 12-well culture plates were purchased from Becton Dickinson Labware (Franklin Lakes, NJ). Human hepatoma cells (Huh-7) and fibroblast-like cell line (NIH3T3) were obtained from RIKEN Bioresource Center (Tsukuba, Japan). Fetal bovine serum (FBS) was purchased from MP Biomedicals, Inc. (Illkirch, France). Renilla Luciferase Assay System Kits were purchased from Promega Co. (Madison, WI). Cell Counting Kit-8 was purchased from Dojindo Laboratories (Kumamoto, Japan). CellLight Lysosomes-GFP and BacMam 2.0 were purchased from Molecular Probes (Eugene, OR).

Synthesis of Poly(β-benzyl-L-aspartate) (PBLA). PBLA was synthesized as previously reported.[8−10] In brief, BLA-NCA (1.2 g, 5 mmol) was dissolved in DMF (2 mL) and diluted with CH_2Cl_2 (20 mL), and *n*-butylamine diluted with CH_2Cl_2 (0.045 mL, 0.045 mmol) was added to initiate ring opening polymerization of NCA. The reaction solution was stirred for 2 days at 35 °C. All procedures were performed under an atmosphere of dry argon. PBLA was precipitated in an excess of *n*-hexane/AcOEt (6:4) and was filtered and dried in vacuo. The polydispersity (M_w/M_n) of PBLA was determined to be 1.06 using a gel permeation chromatography (GPC) system (HLC-8220, TOSOH Co., Tokyo, Japan) equipped with TSKgel columns (SuperAW4000 and SuperAW3000 × 2, TOSOH Co., Tokyo, Japan) and an internal refractive index (RI) detector at 40 °C. NMP containing 50 mM lithium bromide was used as eluent. PEG standards were used for the calibration (data not shown). The ^{1}H nuclear magnetic resonance (NMR) spectrum of PBLA in d_6-DMSO at 80 °C was recorded on a JEOL EX300 spectrometer (JEOL, Tokyo, Japan), and the degree of polymerization was confirmed to be 102 from the peak intensity ratio of methyl protons of the *n*-butyl terminus ($CH_3CH_2CH_2CH_2$–, δ = 0.9 ppm) to aromatic protons of benzyl esters ($C_6H_5CH_2$–, δ = 7.3 ppm; data not shown).

Synthesis of Poly[*N*-(2-aminoethyl)aspartamide] (PAsp(EDA)), Poly{*N*-[*N*′-(2-aminoethyl)-2-aminoethyl]aspartamide} (PAsp(DET)), Poly(*N*-{*N*′-[*N*″-(2-aminoethyl)-2-aminoethyl]-2-aminoethyl}aspartamide) (PAsp(TET)), and Poly[*N*-(*N*′-{*N*″-[*N*‴-(2-aminoethyl)-2-aminoethyl]-2-aminoethyl}-2-aminoethyl)aspartamide] (PAsp(TEP)). N-Substituted polyaspartamides were prepared by aminolysis of PBLA. Lyophilized PBLA (200 mg) was dissolved in NMP (2 mL) and cooled to 0 °C. In another reaction tube, EDA, DET, TET, or TEP (5 mL, 50-fold molar excess over benzyl ester units) was diluted 2-fold with NMP and cooled to 0 °C. The PBLA solution was then added dropwise, and after 1 h reaction 1 N aqueous HCl was added dropwise (5 mL, equimolar concentration to the added amino groups) at <10 °C. Mixtures were then dialyzed (MWCO: 6–8000) at 4 °C against a 0.01 N HCl aqueous solution for 1 day and then against deionized water for an additional day. The final solution was lyophilized to obtain PAsp(EDA), PAsp(DET), PAsp(TET), or PAsp(TEP). In each reaction, quantitative conversion of benzyl ester groups to $-CO-(NHCH_2CH_2)_{1-4}-NH_2$ groups was confirmed using ^{1}H NMR with a polymer concentration of 10 mg/mL D_2O, at 70 °C.

Preparation of mRNA. To perform in vitro transcription (IVT) of GLuc, a protein-expressing fragment of GLuc was cloned into a pSP73 vector (Promega) to give expression under a T7 promoter and then linearized with Nde I for use as an IVT template. IVT was performed using the mMESSAGE mMACHINE T7 Ultra Kit (Ambion, Invitrogen, Carlsbad, CA) according to the manufacturer's protocol. Transcribed mRNA was purified using the RNeasy Mini Preparation Kit (Qiagen, Hilden, Germany), and mRNA concentrations were determined using a spectrophotometer at 260 nm.

Preparation of Polyplexes Containing mRNA. The polycations PAsp(EDA), PAsp(DET), PAsp(TET), or PAsp(TEP) and mRNA were dissolved separately in 10 mM HEPES buffer. The concentration of nucleic acid was set at 50 μg/mL, and that of polycation was adjusted at the residual molar ratio of the polycation amino groups to mRNA phosphate groups (N/P) = 10. Solutions of polycation and mRNA were mixed at a ratio of 1:2 to obtain polyplex solutions with a final mRNA concentration of 33.3 μg/mL. ExGen 500/mRNA polyplex solution was prepared according to the manufacturer's protocol. Size and ζ-potential measurements of mRNA polyplexes were carried out using Zetasizer nanoseries (Malvern Instruments Ltd., Worcestershire, U.K.). For measuring polyplex size, a small glass cuvette (ZEN2112, Malvern Instruments Ltd.) was used. The obtained data were analyzed by using a cumulant method, and the hydrodynamic diameter of the polyplex was calculated with the Stokes–Einstein equation. For ζ-potential measurement, a folded capillary cell (DTS 1060, Malvern Instruments Ltd.) was used. The ζ-potential was calculated from the obtained electrophoretic mobility by applying the Smoluchowski equation.

Transfection of mRNA Polyplexes toward Huh-7 Cells. Huh-7 cells were cultured in DMEM containing 10% FBS at 37 °C in a humidified atmosphere containing 5% CO_2. For transfection, the cells were seeded onto 96-well culture plates (2500 cells/well) and were incubated overnight in DMEM containing 10% FBS (100 μL). Prior to transfection, the medium was replaced with an equal volume of fresh medium. Polyplex solutions containing mRNA were then added to each well (250 ng of mRNA/well). GLuc expression was evaluated according to photoluminescence intensity using the Renilla Luciferase Assay System and a Luminometer Glomax 96 (Promega Co.) from 3 to 72 h after transfection (n = 4). Cytotoxicity was assessed using a Cell Counting Kit-8 according to the manufacturer's protocol. Data are presented relative (%) to values from nontransfected control cells (n = 4).